Journal of Molecular Liquids 372 (2023) 121182

Contents lists available at ScienceDirect

Journal of Molecular Liquids

journal homepage: www.elsevier.com/locate/molliq

Enhanced sensible heat storage capacity of nanofluids by improving the photothermal conversion performance with direct radiative absorption of solar energy

Oguzhan Kazaz [a], Nader Karimi [a,b], Shanmugam Kumar [a], Gioia Falcone [a], Manosh C. Paul [a,*]

[a] Systems, Power & Energy Research Division, James Watt School of Engineering, University of Glasgow, Glasgow, G12 8QQ, the United Kingdom of Great Britain and Northern Ireland
[b] School of Engineering and Materials Science, Queen Mary University of London, London, E1 4NS, the United Kingdom of Great Britain and Northern Ireland

ARTICLE INFO

Article history:
Received 19 October 2022
Revised 28 December 2022
Accepted 29 December 2022
Available online 2 January 2023

Keywords:
Solar energy
Nanofluids
Photothermal energy conversion and storage
Solar energy materials
Brownian motion
Solar absorption
Collision
Direct absorption

ABSTRACT

The paper numerically investigates the fluid flow and radiative heat transfer behaviour of water-based mono and hybrid nanofluids in a direct absorption solar collector under solar irradiation boundary conditions. The effects of radiation on the heat and flow performance with operating parameters such as the type of nanoparticles, volume concentrations of nanoparticles, nanoparticle size and type of base fluids are investigated. The numerical results reveal that uniform temperature distribution is obtained with an incident radiation of 1029.81 W/m^2 and that the collector performance increases with the addition of nanoparticles owing to their higher radiative properties. While the temperature gain for pure water is 5.58 K, it is estimated to be 48.72 K and 51.32 K with the volume concentrations of 70 ppm and 100 ppm for Al + Al_2O_3 and Al + Graphite nanofluids, respectively. Moreover, the thermal performance of the collector is positively affected by increasing the size of nanoparticle. For example, for Al + Al_2O_3 nanofluids at 10 ppm volume concentration, the temperature increase is 37.12 K and 42.02 K at 10 nm and 50 nm, respectively. Therefore, hybrid nanofluids can be considered as effective heat transfer fluids to increase the solar radiation absorbability, and subsequently, improve the efficiency and performance of the direct absorption solar collector.

1. Introduction

Increasing urbanization and industrialization with the rise in the world's population and general living standards have significantly elevated the need for energy [1]. However, dependency upon fossil fuels, as energy sources, highly intensifies the emission of greenhouse gases resulting in serious concerns about global warming [2,3]. This has highlighted renewable energy generation as an essential perquisite for sustainability [4]. The ubiquitous nature of solar energy along with its relative ease of use makes it a very attractive source of renewable energy [3,5].

The solar irradiation can be harnessed by converting solar energy into thermal energy through solar collectors [6]. To do so, solar radiation needs to be collected optimally. In conventional solar collectors, solar radiation is concentrated and converted in to heat. This is then transferred to a heat transfer fluid. In this indirect heat transfer process, the collector performance drops as the temperature difference between the heat transfer fluid and the absorber increases the heat losses [7]. To address this issue, solar radiation is directly absorbed by the heat transfer fluid, and solar radiation is converted into heat by using direct absorption solar collectors [8]. Here, the heat transfer fluid also acts as an absorbent medium, causing smaller temperature difference and thus enhancing the performance and efficiency of the collector.

Nonetheless, standard fluids, such as water, are incapable of absorbing enough sunlight because of their low absorption properties. Therefore, adding nanoparticles to the working fluids is a good way to increase optical properties of the working fluid because of the absorption and scattering characteristics of nanoparticles. Additionally, the thermophysical properties of the base fluid can be enhanced by adding nanoparticles [9,10]. Song *et al.* [11] used Rayleigh scattering and Mie scattering theories to find the optical properties of Al_2O_3 nanofluid after aggregation. They claimed that the particle size distribution resulting in aggregation affected the optical properties of the nanofluid, and smaller particle size also induced a larger absorption coefficient. Chen *et al.* [12] investigated the optical properties of Au nanofluids with different sizes in cube shaped and flat shaped. Au nanofluids showed better photothermal conversion properties than base fluids at low fraction.

* Corresponding author.
E-mail address: Manosh.Paul@glasgow.ac.uk (M.C. Paul).

https://doi.org/10.1016/j.molliq.2022.121182
0167-7322/

Nomenclature

L	Length of the collector (m)
H	Height of the collector (m)
AR	Aspect ratio
I_λ	Radiation intensity (W/m^{2}μm)
$\vec{r}$	Position vector
$\vec{s}$	Direction vector
$I_{b\lambda}$	Black body intensity (W/m^{2}μm)
n	Refractive index
$\vec{s}'$	Scattering direction vector
$Q_{e\lambda}$	Extinction efficiency
k	Absorption index
n	Refractive index
f_v	Particle volume fraction
q	Heat flux (W/m^2)
D	Diameter of the particle (m)
m	Normalized refractive index of the particle to the fluid
α	Size parameter
$Q_{s\lambda}$	Scattering efficiency
$K_{e\lambda}$	Extinction coefficient (1/m)
$K_{a\lambda}$	Absorption coefficient (1/m)
$K_{s\lambda}$	Scattering coefficient (1/m)
C_p	Specific heat (J/kgK)
k	Thermal conductivity (W/mK)
h	Convective heat transfer coefficient (W/m^{2}K)
r	Radius of the nanoparticle
u, v	Velocity vectors (m/s)
p	Pressure (Pa)
g	Gravitational acceleration (m/s^2)
T	Temperature (K)
T_0	Initial temperature (K)
$Q_{a\lambda}$	Absorption efficiency
N_θ	Theta division
N_φ	Phi division
E	Enhancement
ΔH	Enthalpy change (J/kg)
ΔT	Temperature change (K)
Nu	Nusselt number
Ra	Rayleigh number

Greek symbols

ρ	Density (kg/m^3)
μ	Dynamic viscosity (Ns/m^2)
β	Thermal expansion coefficient (1/K)
σ	Stefan-Boltzmann (5.67×10^{-8} W/m^{2}K^4)
ε	Emissivity
φ	Nanoparticle fraction
λ	Wavelength of incident light (μm)
Φ	Phase function
Ω'	Solid angle
k_B	Boltzmann constant (1.3807×10^{-23} J/K)

Subscripts

nf	Nanofluid
p	Nanoparticle
f	Base fluid
amb	Ambient
hnf	Hybrid nanofluid
eff	Effective
1	First nanoparticle
2	Second nanoparticle
s	Stored
h	Hot
c	Cold
$conv$	Convective
rad	Radiative
s_1, s_2	Solid nanoparticles

The cubic model was found to have a higher photo-thermal conversion efficiency than the flat model by using the same working fluids. Because of the interaction of the optical properties of the liquid, the efficiency of the photo-thermal conversion for flat model declined, but with increasing Au dimensions. The Au nanofluid with a particle size of 25 nm particularly offered higher absorbance characteristic than 33 nm and 40 nm sized particles. Du and Thang [13] theoretically calculated the extinction coefficient of Ag/water based nanofluids using particles agglomerated by considering multiple scattering and dependent scattering. By using diffusion limited cluster aggregation (DLCA) simulation and generalized multi-particle Mie solution (GMM) methods, the effects of particle size, particle agglomeration and particle volume fraction on the extinction co-efficient of nanofluids with particle agglomeration were investigated. While the extinction coefficient increased at long wavelengths, there was a small decrease in absorption at short wavelengths.

Besides, Said *et al.* [14] experimentally and analytically studied the optical properties of water-based metal oxide (Al_2O_3 and TiO_2) nanofluids with two different volume fractions (0.1 % and 0.3 %) by using Rayleigh scattering theory. TiO_2 nanofluids' extinction co-efficient and refractive index were discovered to be higher in the visible light region than Al_2O_3 nanofluids. Menbari *et al.* [15] investigated the effects of pH value, surfactant fraction and sonication time with using CuO and γ-Al_2O_3 nanoparticles. They experimentally and analytically examined the extinction coefficients of mono and binary nanofluids. They found that the blended nanoparticle's extinction coefficient is sum of its components' extinction coefficients, and the extinction coefficient increased with increasing volume concentration of nanoparticles. He *et al.* [16] experimentally analysed the photothermal properties of Cu-H_2O nanofluids. They examined particle size, pH, optical depth, and mass fraction that affect the nanofluids' transmittance. According to their results, transmittance of nanofluids decreased with increasing optical path, mass fraction and particle diameter and transmittance of deionized water was higher than nanofluids. The maximum temperature of the nanofluids with 0.1 % volume fraction increased to 25.3 % compared to deionized water. Karami *et al.* [17] prepared water based alkaline functionalized carbon nanotubes (f-CNT) nanofluid as the working fluid. Experimental results showed that with the addition of 150 ppm f-CNT, the extinction co-efficient of pure water increased by about 4.1 cm^{-1}, and the thermal conductivity enhanced by 32.2 %. Thermal conductivity also increased with increasing volume concentration and temperature.

Furthermore, Menbari *et al.* [18] experimentally analysed the effects of pH, surfactant fraction and ultrasonic time on the stability of nanofluids. Ethylene glycol and ethylene glycol–water mixture were used as base fluid. The experimental results showed that the optimal pH values of 6.5–7.5, 8.5–10, 7–8.2; optimal surfactant concentrations of 0.25–0.5, 1.65, and 1.5; and optimal sonication times of 55, 120, and 100–120 min were found for the ethylene glycol-based Al_2O_3, ethylene glycol-based CuO, and ethylene glycol-based Al_2O_3–CuO, respectively. The optimal pH value, surfactant concentrations and sonication time of ethylene glycol–

water based Al_2O_3-CuO were 7.2–8.5, 1.35, and 100–120 min, respectively. Zhang *et al.* [19] examined the effects of water-based Au, Si, Fe_3O_4 and Al_2O_3 nanofluids on their photothermal conversion properties. The experimental results showed that nanofluids increased photothermal conversion efficiency and the efficiency enhanced in the order of Al_2O_3, Fe_3O_4, Si and Au. The photothermal conversion efficiency was found to increase non-linearly with concentration for all nanofluids. Zhang *et al.* [20] experimentally and theoretically investigated the radiative properties of the ionic liquid [HMIM][NTf_2] and its nanofluids. The extinction coefficient of the Ni nanofluid with an average diameter of 40 nm for the volume concentration of 10 ppm was higher Cu nanofluid with a similar average diameter because of the different refractive indices. When the volume concentration increased to 40 ppm, the energy fraction absorbed by the Ni/C nanofluid almost reached 100 % after the incident light was exceeded by only 1 cm.

Moreover, Otanicar *et al.* [21] experimentally and numerically investigated photothermal conversion efficiencies of different water based nanofluids; graphite, carbon nanotubes and silver. The effects of nanoparticle size and volume concentration were studied. The results showed that up to 5 % enhancement in efficiency was observed in direct absorption solar collectors by applying nanofluids under flow conditions as the absorption mechanism. Turkyilmazoglu [22] analytically investigated an increase in the thermal efficiency of the collector by using Al_2O_3/water nanofluid as 2D and steady state. Two different boundary conditions, non-adiabatic and isothermal wall conditions, were applied on the base panel of the collector channel. It was found that the thermal efficiency of the solar collector increased by increasing the new physical parameters compared to the conventional adiabatic wall condition, depending on the increase in the final outlet mean temperature. The thermal efficiency of the collector for the non-adiabatic bottom panel was 85.63 % with Al_2O_3/water nanofluid. In isothermal base panels, on the other hand, 100 % efficiency was obtained faster with lower base temperatures at higher nanoparticle volume concentrations. Gupta *et al.* [23] experimentally examined the effect of Al_2O_3 nanoparticles with a volume concentration of 0.005 % and a size of 20 nm at three different flow rates of 1.5, 2, 2.5 lpm. An increase of 8.1 % and 4.2 % was observed in the collector efficiency at 1.5 and 2 lpm flow rates of the nanofluid, respectively. The optimum flow rate for maximum collector efficiency was found to be 2.5 and 2 lpm at different flow rates for water and nanofluid, respectively.

There is also numerical analysis in which the optical and radiative properties of the heat transfer fluid are not considered in direct absorption solar collectors but only the effects of natural convection are examined. For instance, Hatami and Jing [24] carried out finite element and response surface methods in order to analyse the performance a collector with a wavy wall using Al_2O_3/water nanofluid as a heat transfer fluid. The bottom wavy wall was at constant temperature whereas the top wall was under a constant heat flux condition due to solar energy, and side walls were insulated. Nine different cases were simulated as a combination of wave amplitude and wave numbers in order to investigate the best response. The results indicated that the best mean Nusselt number was obtained with the lowest wave amplitude (0.02) and average wave number (4.00). On the other hand, Alsabery et al. [25] studied the heat transfer behaviour of wavy top surface collector using a water based Al_2O_3 nanofluid. The effects of oscillations, wave amplitude, particle concentration, and Rayleigh number were examined. Their findings revealed that as the oscillations improved, the higher temperature gradients were obtained. The mean Nusselt number was found to enhance with increasing particle volume concentration as a result of improved thermal conductivity. It was further observed that conduction was more dominant than convection at low Rayleigh numbers. However, an augmentation in local heat transfer was noticed when the wave amplitudes and wave number were increased. Hatami and Jing [26] also investigated the impacts of water based TiO_2, Al_2O_3, and CuO nanofluids on two different bottom wall configurations. The outcomes indicated that the highest local and average Nusselt numbers were achieved from wavy and flat walls, respectively. The best average Nusselt number was also obtained using water based TiO_2 nanofluid.

As indicated by the literature review, studies on stationary fluids generally focus on the thermal and optical properties of mono nanofluids. Therefore, there is a lack of information about the heat storage and heat transfer performances of nanofluids on directly heated solar collectors and it is a matter of curiosity how the effects of combined radiative and natural convection will be as a result of the heat transfer fluid being heated by the sunbeam in closed cavities, so more investigations are still needed to analyse these combined effects. Besides, because the nanoparticles in the radiation environment cause either a decrease or an increase in the energy due to scattering, the direction of energy transfer from the radiation may change. Thus, it is estimated that the heat transfer and flow characteristics of the working fluid would change inside the solar collector. Furthermore, comparisons have been made generally considering mono nanoparticles. The effects of hybrid nanofluids, which can be considered as a new type of heat transfer fluid in recent years, on the thermal performance of direct absorption solar collectors, however, are still not well understood, and there is a major research gap identified in this area. Importantly, as different types of nanoparticles have different optical properties, the effects of them on the thermal system are still unknown.

Furthermore, it is noteworthy that most of the studies in the literature only used a very limited range of nanoparticle sizes. However, it is expected that the effects of nanoparticle size on the thermal and storage performances of the collector would be different as they would affect the optical and thermophysical properties. In addition to the nanoparticle size, volume concentration of nanoparticles could affect the absorption and scattering of heat transfer fluid. Since the volume concentration impacts the optical properties as well as the Brownian motion of the nanoparticles, there is a need to investigate the effects of the concentration on the system. Moreover, it is seen that water is generally used as a base fluid in the previous studies. The fact that ethylene glycol and Therminol VP-1 heat transfer fluids, which can be considered as a new type of base fluid, have received almost no attention. This paper for the first-time emphasise their importance with a comparative analysis. Given these, the overall aim of the current study is to shed light on the effects of radiation upon heat transfer in a directly heated solar collector for photo-thermal conversion and storage, and numerical simulations are used to conduct an in-depth parametric study within the given frameworks.

2. Problem statement and mathematical formulation

Fig. 1(a) shows a nanofluid-based direct absorption solar collector with a height H and a length L. The aspect ratio of collector is defined by L/H. In the literature, the aspect ratio of the collectors is variable between 5 and 833 [12,27,21,28,29,30]. As stated in the references, the aspect ratio of $AR = 10$ has been selected as the initial value for the current study. The transparent glass covering the top surface of the collector allows most of the sunbeam coming vertically to pass through. When photothermal energy acts on nanoparticles of the same shape and size dispersed in the base fluid (Fig. 1(b)), they begin to trap this energy due to the radiative properties of nanoparticles. Thus, the nanoparticles interacting by colliding with each other increase the temperature of the nanofluid

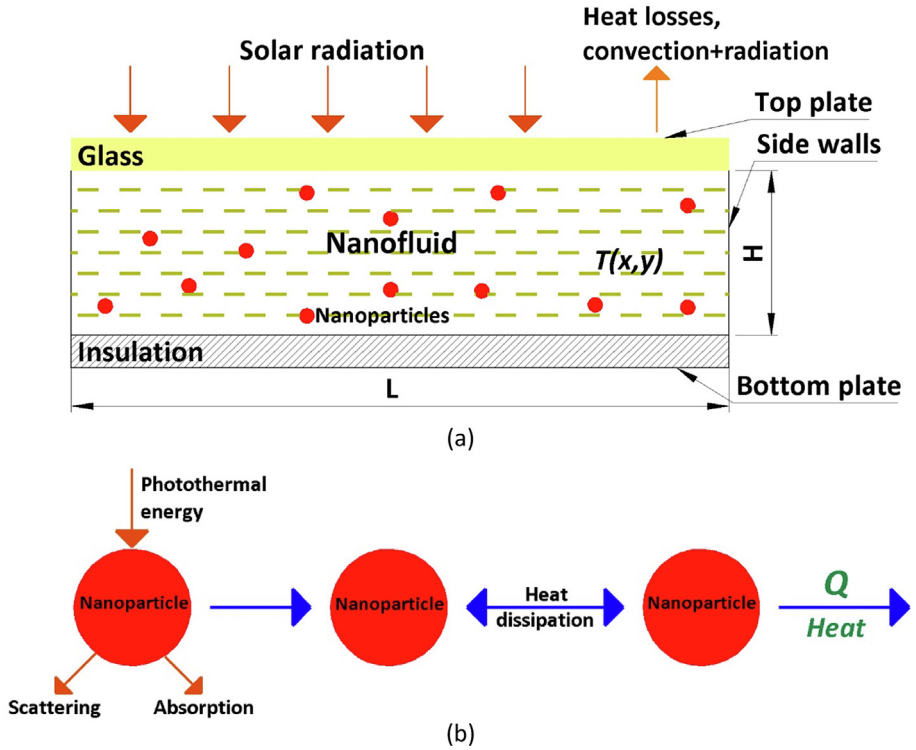

Fig. 1. (a) A 2D schematic diagram of a direct absorption solar collector, (b) behaviour of nanoparticles under photothermal energy conversion inside the collector.

as a result of heat dissipation. It is assumed that the top surface is exposed to the atmosphere. Because of the absorption of solar energy, the nanofluid heats up and some heat is lost from the solar collector by convection and radiation. Because it is used as a storage cavity, the bottom and side walls are considered adiabatic, and in order to further increase the heat storage gain of the fluid, these walls are defined as highly reflective and the radiation that is transferred to the walls is reflected to the inside of the collector. Finally, a two-dimensional heat transfer and fluid flow numerical model is developed to analyse this configuration.

The Radiation Transport Equation (RTE) in a participating medium is solved to evaluate the spectral attenuation of radiation within the translucent nanofluid depth after the radiative properties are calculated. The general form of RTE is given by [31]:

$$\nabla\cdot\left(I_\lambda\left(\vec{r},\vec{s}\right)\vec{s}\right)+(K_{a\lambda}+K_{s\lambda})I_\lambda\left(\vec{r},\vec{s}\right)=K_{a\lambda}n^2I_{b\lambda}+\frac{K_{s\lambda}}{4\pi}\int_0^{4\pi}I_\lambda\left(\vec{r},\vec{s}'\right)\Phi\left(\vec{s}\cdot\vec{s}'\right)d\Omega' \quad (1)$$

where $\Phi\left(\vec{s}\cdot\vec{s}'\right)$ is the scattering phase function and describes the probability that a ray from one direction $\vec{s}$, will be scattered into a certain other direction $\vec{s}'$. It can be approximated using spectral blackbody distribution ($I_{b\lambda}$), assuming that solar radiation normally enters the cavity.

For pure fluids, the scattering effects of the base fluid can be neglected because absorption dominates attenuation. Therefore, only absorption can be considered, and the extinction co-efficient is calculated as [27]:

$$K_{e\lambda,f}=K_{a\lambda,f}=\frac{4\pi k}{\lambda} \quad (2)$$

For nanofluids, however, the attenuation is caused by both absorption and scattering because of the presence of nanoparticles. Therefore, the volumetric medium can be affected by several factors such as nanofluid volume fraction, type of base fluid, type of nanoparticle and size. In the scattering regime of the particulate medium defined by Tien and Drolen [32], it has been shown that nanoparticles exhibit independent scattering, and this regime can also be applied when the fraction of nanoparticle is less than 0.6 %. Rayleigh scattering can be well-applied as nanofluids affect absorption as well as the scattering of small particles. The Rayleigh scattering approach to investigate the optical properties also exists for small particles [33,28,34].

According to Rayleigh scattering, the extinction coefficient can be given by [27]:

$$K_{e\lambda,p}=\frac{3f_v Q_{e\lambda}(\alpha,m)}{D} \quad (3)$$

m and α can be given as [27]:

$$m=\frac{m_{particles}}{n_{fluid}} \quad (4)$$

$$m_{particles}=n+ik \quad (5)$$

$$\alpha=\frac{\pi D}{\lambda} \quad (6)$$

where n and k are the refractive and absorption indices of nanoparticle, respectively. The optical properties are found in the literature [35–39].

The extinction efficiency can be defined as [40]:

$$Q_{e\lambda}=Q_{a\lambda}+Q_{s\lambda} \quad (7)$$

where

$$Q_{a\lambda}=4\alpha Im\left\{\frac{m^2-1}{m^2+2}\left[1+\frac{\alpha^2}{15}\left(\frac{m^2-1}{m^2+2}\right)\frac{m^4+27m^2+38}{2m^2+3}\right]\right\} \quad (8)$$

$$Q_{s\lambda}=\frac{8}{3}\alpha^4\left|\left(\frac{m^2-1}{m^2+2}\right)\right|^2 \quad (9)$$

If Equations (6) and (7) are substituted in Equation (3), the following expression can be obtained for $K_{e\lambda}$.

$$K_{e\lambda} = K_{a\lambda} + K_{s\lambda} \tag{10}$$

where

$$K_{a\lambda} = \frac{12\pi f_v}{\lambda} Im\left\{\frac{m^2-1}{m^2+2}\left[1+\frac{\pi^2 D^2}{15\lambda^2}\left(\frac{m^2-1}{m^2+2}\right)\frac{m^4+27m^2+38}{2m^2+3}\right]\right\} \tag{11}$$

$$K_{s\lambda} = \frac{8\pi^4 D^3 f_v}{\lambda^4}\left|\left(\frac{m^2-1}{m^2+2}\right)\right|^2 \tag{12}$$

The effective extinction coefficient of the nanofluid can be proposed as the sum of both the base fluid and the nanoparticle's extinction coefficient:

$$K_{e\lambda,nf} = K_{e\lambda,p} + K_{e\lambda,f} \tag{13}$$

In addition, the total extinction coefficient of the hybrid nanofluids can be assumed by adding the extinction coefficient of each form of the based fluid and nanoparticles [41]:

$$K_{e\lambda,hybridnf} = K_{e\lambda,f} + K_{e\lambda,p1} + K_{e\lambda,p2} \tag{14}$$

Nanofluid in the cavity is considered to be incompressible and Newtonian, and flow is considered to be in laminar and steady state. Moreover, the fluid phase and nanoparticles are assumed to be in thermal equilibrium, and they flow with the same velocity. The nanoparticles are also supposed to be of uniform spherical shape and size. The thermophysical properties of the nanoparticles are given in Table 1. The thermophysical properties of the nanofluid are assumed to be constant except for the density, which is based on the Boussinesq approximation. The extinction coefficient of the heat transfer fluid is also approximated to be equal to the average extinction coefficient in the visible and near infrared region [42].

Because of these assumptions, the dimensional governing equations in the Cartesian coordinate system for the fluid flow and heat transfer for the single-phase model can be expressed as,

Continuity equation:

$$\frac{\partial u}{\partial x} + \frac{\partial v}{\partial y} = 0 \tag{15}$$

x-momentum equation:

$$u\frac{\partial u}{\partial x} + v\frac{\partial u}{\partial y} = -\frac{1}{\rho_{nf}}\frac{\partial p}{\partial x} + \frac{\mu_{nf}}{\rho_{nf}}\left(\frac{\partial^2 u}{\partial x^2} + \frac{\partial^2 u}{\partial y^2}\right) \tag{16}$$

y-momentum equation:

$$u\frac{\partial v}{\partial x} + v\frac{\partial v}{\partial y} = -\frac{1}{\rho_{nf}}\frac{\partial p}{\partial y} + \frac{\mu_{nf}}{\rho_{nf}}\left(\frac{\partial^2 v}{\partial x^2} + \frac{\partial^2 v}{\partial y^2}\right) + \frac{(\rho\beta)_{nf}}{\rho_{nf}} g(T - T_0) \tag{17}$$

Conservation of energy:

$$\rho_{nf} C_{p_{nf}}\left(u\frac{\partial T}{\partial x} + v\frac{\partial T}{\partial y}\right) = k_{nf}\left(\frac{\partial^2 T}{\partial x^2} + \frac{\partial^2 T}{\partial y^2}\right) - \nabla \cdot q_r \tag{18}$$

The conservation of energy is coupled with the RTE, and the divergence of the radiative heat flux is calculated as [47]:

$$\nabla \cdot q_r = K_{a\lambda}\left[4\pi I_{b\lambda} - \int_0^{4\pi} I_\lambda\left(\vec{r},\vec{s}'\right) d\Omega'\right] \tag{19}$$

The thermal boundary conditions are presented as:

at all the solid boundaries:

$$u = v = 0 \tag{20}$$

at the top cover:

$$q = h(T - T_{amb}) + \varepsilon\sigma(T^4 - T_{amb}^4) \tag{21}$$

at the vertical walls:

$$\frac{\partial T}{\partial x} = 0 \tag{22}$$

at the bottom wall:

$$\frac{\partial T}{\partial y} = 0 \tag{23}$$

The convection heat transfer coefficient, $h = 19.532 Wm^{-2}K^{-1}$, is determined as a function of wind speed by means of the Duffie correlation [48]:

$$h = 5.7 + 3.8v \tag{24}$$

The density, specific heat, and thermal expansion coefficient of the nanofluid are defined as [49]:

$$\rho_{nf} = \rho_f(1-\varphi) + \rho_p\varphi \tag{25}$$

$$(\rho C_p)_{nf} = (\rho C_p)_f(1-\varphi) + (\rho C_p)_p\varphi \tag{26}$$

$$(\rho\beta)_{nf} = (\rho\beta)_f(1-\varphi) + (\rho\beta)_p\varphi \tag{27}$$

where β_f and β_p are the thermal expansion coefficients of the base fluid and the nanoparticle, respectively.

The density, specific heat, and thermal conductivity of the hybrid nanofluid are modified and defined as [50]:

$$\rho_{hnf} = \varphi_{p1}\rho_{p1} + \varphi_{p2}\rho_{p2} + (1-\varphi)\rho_f \tag{28}$$

where φ is the overall volume concentration of two different types of nanoparticles dispersed in hybrid nanofluid and is calculated as:

$$\varphi = \varphi_{p1} + \varphi_{p2} \tag{29}$$

$$(\rho C_p)_{hnf} = \varphi_{p1}\rho_{p1}C_{p,p1} + \varphi_{p2}\rho_{p2}C_{p,p2} + (1-\varphi)\rho_f C_{p,f} \tag{30}$$

$$(\rho\beta)_{hnf} = \varphi_{p1}\rho_{p1}\beta_{p1} + \varphi_{p2}\rho_{p2}\beta_{p2} + (1-\varphi)\rho_f\beta_f \tag{31}$$

The thermal conductivity of the nanofluid is defined as

$$k_{eff} = k_{static} + k_{Brownian} \tag{32}$$

The static thermal conductivity of nanofluid is defined as [51]:

$$k_{static} = k_f\frac{k_p + 2k_f - 2\varphi(k_f - k_p)}{k_p + 2k_f + \varphi(k_f - k_p)} \tag{33}$$

Table 1
Thermophysical properties of nanoparticles [43–46].

Properties	Cu	Au	Al	Al_2O_3	Graphite
ρ (kg/m^3)	8954	19,320	2700	3970	2210
C_p (J/kgK)	383	128.8	900	765	709
k (W/mK)	400	314.4	247	40	1950

where k_f and k_p are the thermal conductivities of the base fluid and the nanoparticle, respectively.

The static thermal conductivity of the hybrid nanofluid can be modified as [52],

$$(k_{hnf})_{static} = k_{bf}\frac{k_{s2} + 2k_{bf} - 2\varphi_2(k_{bf} - k_{s2})}{k_{s2} + 2k_{bf} + \varphi_2(k_{bf} - k_{s2})} \tag{34}$$

where

$$k_{bf} = k_f\frac{k_{s1} + 2k_f - 2\varphi_1(k_f - k_{s1})}{k_{s1} + 2k_f + \varphi_1(k_f - k_{s1})} \tag{35}$$

k_{bf} is the thermal conductivity of the first nanofluid, whereas k_f is the thermal conductivity of the base fluid.

The Brownian thermal conductivity is calculated as [53]:

$$k_{Brownian} = \frac{\rho_p\varphi C_{p,p}}{2}\sqrt{\frac{k_B T}{3\pi r\mu_f}} \tag{36}$$

The effective viscosity of the nanofluid is defined as [54]:

$$\mu_{nf} = \mu_f(1 + 39.11\varphi + 533.9\varphi^2) \tag{37}$$

In order to calculate the effective viscosity of the nanofluid, φ is the volume concentration of each nanoparticle while φ must be the overall volume concentration of nanoparticles used to define the hybrid nanofluid [55–57].

The useful heat that the nanofluid gains in the direct absorption solar collector can be obtained by [58]:

$$q_{usefulheat} = C_p\Delta T \tag{38}$$

Finally, the stored energy is determined from [59,60]:

$$q_s = \Delta H \tag{39}$$

where ΔT and ΔH are the temperature change and enthalpy deviation of the nanofluid, respectively. The temperature of the nanofluid increases from low (initial) temperature to high (final) temperature by heating with the effect of solar energy. The enthalpy change is also equivalent to the total enthalpy deviation of the nanofluid across the state as a thermodynamic point of view.

Furthermore, in order to find the enhancement of the thermal performance of direct absorption solar collector between the case of the pure fluid and adding nanoparticles case, the enhancement can be defined as:

$$E = \frac{(thermal\,variable)_{nanofluid} - (thermal\,variable)_{purefluid}}{(thermal\,variable)_{purefluid}} \tag{40}$$

where the thermal variable indicates here either the useful heat or stored energy.

3. Numerical procedures

The governing equations and boundary conditions are solved by using a pressure-based finite volume method solver in ANSYS Fluent 2020 R1. The radiative transfer equation is solved by the Discrete Ordinates (DO) method. The effects of absorbing, emitting, and scattering elements are included. The DO method is the directional variation of the radiation intensity and the transfer equation for a set of discrete directions is solved by spanning the range of 4π total solid angles [61]. The DO method divides the radiation spectrum into wavelength bands, and the RTE is integrated in each wavelength range. Theta Divisions (N_θ) and Phi Divisions (N_φ) are used to discretise each octane of the angular space and describe the number of control angles. ANSYS Fluent can only solve 4 octants for a 2D heat transfer and fluid flow due to symmetry, hence a total of $4N_\theta N_\varphi$ directions $\vec{s}$ is solved [31]. By transforming the DO model Equation (1) into a transport equation for radiation in spatial co-ordinates, the radiative transfer equation is analysed as a field equation and then solved for a finite number of separate solids [31]. The SIMPLE algorithm is provided for the velocity–pressure coupling. All equations are discretised by the second-order upwind differencing scheme. Least Squares Cell Based and PRESTO! are adapted for gradient and pressure, respectively. The convergence criteria show that the residuals of the momentum and continuity equations are below 10^{-5} and for the energy and DO equations they are below 10^{-6}. 5x5 divisions are used for each octant of angular space along the polar and azimuth extensions to discretise the radiative transfer equation to better resolve the effects of geometric properties and spatial changes in temperature and to obtain more accurate results, and 3x3 pixelization is also used to account for any control volume overhang [31].

3.1. Grid independence test

A grid refinement test is necessary for reliable numerical simulations. The non-uniform mesh used is presented in Fig. 2. The grid sensitivity results of volumetric absorbed radiation, radiation temperature and right wall shear stress with different mesh volumes for Al/water nanofluid with volume fraction of 0 ppm (no nanoparticle effect) and 100 ppm (observed nanoparticle effect, d = 10 nm) are shown in Fig. 3. Four different mesh systems with the total number of 36000, 64000, 100000, 144,000 cells are considered. The mesh number at fluid domain is increased so that the fluid flow and heat transfer fields can be accurately resolved. As can be seen in Fig. 3, there are no changes for the 0 ppm with different mesh numbers. However, after exceeding 64,000 cells, it can be clearly seen that similar results for 100 ppm are obtained. Therefore, the results obtained by the grid consisting of 64,000 cells can be considered grid independent as the deviation with the results for the three higher resolution mesh sizes is only ± 0.01 %.

3.2. Model validation

The experimental and numerical study conducted by Otanicar et al. [21] is selected to validate the radiative heat transfer and nanoparticle models. Fig. 4 compares the results for stagnation temperature differences and collector efficiency of water-based different nanoparticles as a function of volume fraction. The direct absorption solar thermal collector is used with a mass flow rate of 42 *ml/h*. The top boundary condition of the collector is considered as convective and there is a radiative heat transfer with $h = 23Wm^{-2}K^{-1}$. The top wall is exposed to solar radiation with $1000W/m^2$. As shown in Fig. 4, the simulation results match well with benchmark model. As shown in Fig. 4(a), the minimum and maximum errors are 0.31 % and 11 %, respectively. In Fig. 4(b), the minimum and maximum errors are also 1.03 % and 10.27 % for 0 % Graphite/water and 0.05 % Graphite/water nanofluids, respectively.

Another model validation is performed with numerical studies on natural convection conducted by Ho et al. [62]. The enclosure cavity is filled with water-based Al_2O_3 nanoparticles with a volume concentration of 4 %, with an aspect ratio of 1, Prandtl number of 6.2 and at the Rayleigh number of 10^4, 10^5 and 10^6. The top and bottom walls of the cavity are adiabatic while the sidewalls are kept at constant hot T_h and cold T_c temperatures. They proposed the correlation of $\bar{Nu}_{h,f} = C(1 + \varnothing)^m Ra_f^n$ to calculate the mean Nusselt number at the hot wall where C is the co-efficient, and m and n are the components. Table 2 shows the mean convective Nusselt numbers on the hot wall, which also match closely with the benchmark model. As seen in Table 2, whereas the maximum error is

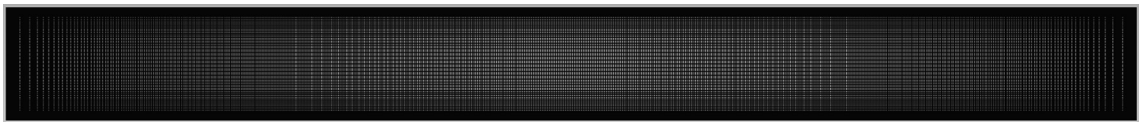

Fig. 2. 2D generated mesh structure.

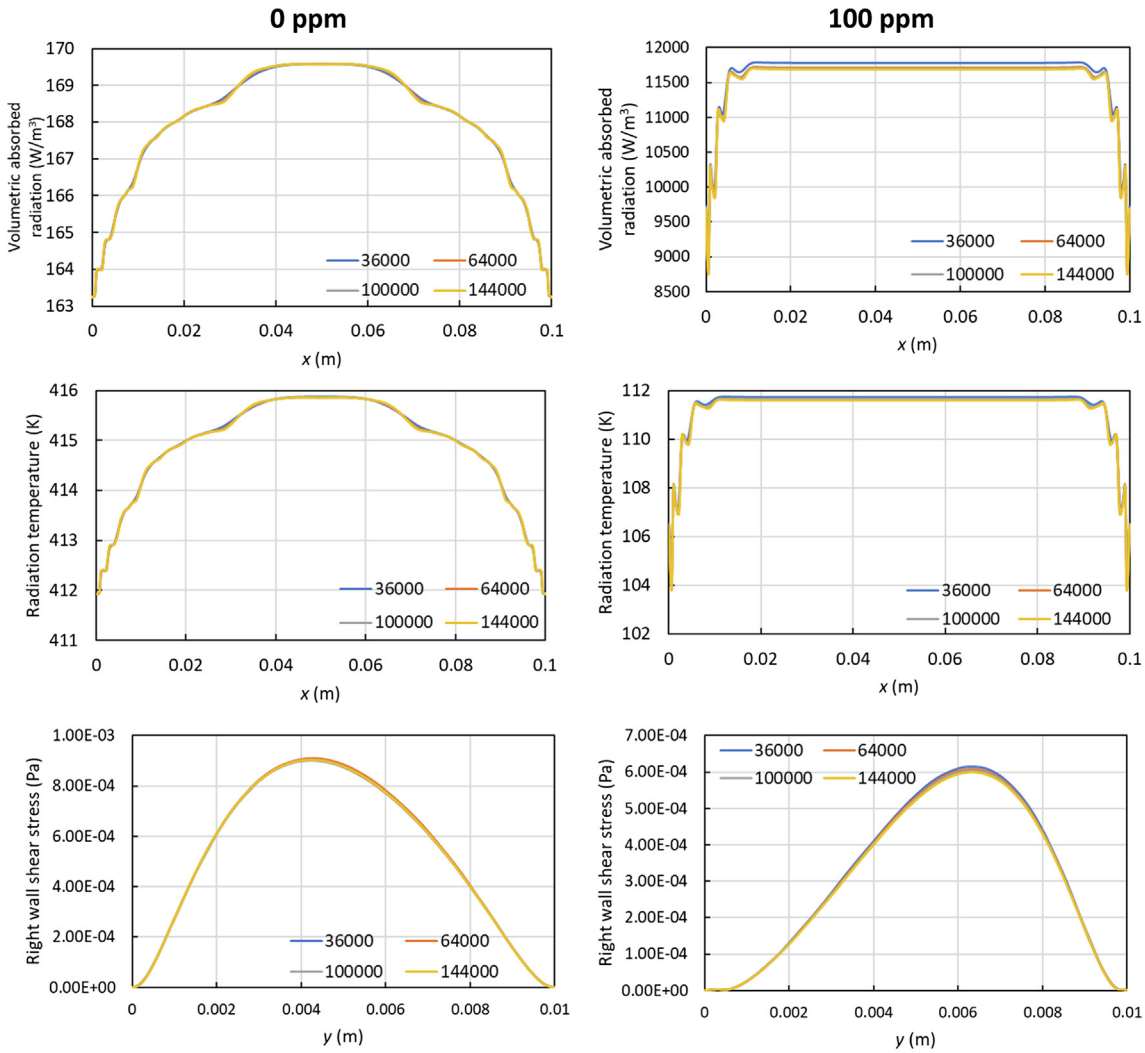

Fig. 3. Variations of volumetric absorbed radiation and radiation temperature along horizontal midline, and right wall shear stress with four different grid numbers.

4.89 % at the Rayleigh number of 10^4, the minimum error is 0.21 % at the Rayleigh number of 10^5 and 10^6.

4. Results and discussion

This part focusses on the effects of nanoparticle type and volume concentration, particle diameter, and base fluid type that can affect the photo-thermal conversion and thermal energy storage performances of the closed-based solar collector system.

4.1. Effects of volume concentration of nanofluids

In this section, the effects of variation in the volume concentration of nanoparticles are investigated using Graphite nanoparticles with different volume fractions of 0 ppm, 4 ppm, 7 ppm, 10 ppm, 40 ppm, 70 ppm and 100 ppm. With increasing the volume fraction of nanoparticles, the nanofluid absorbs more solar radiation, resulting in sudden increases in the temperature of the collector. As shown in Fig. 5(a), the extinction coefficient increases with rising volume fraction, and this result is consistent with the study of Menbari et al. [15]. Therefore, as the radiation absorption capacity of the nanofluid increases, the average temperature of the fluid in the collector and the average volumetric heat generated by the radiation also increases.

As further shown in Fig. 5(a), while the maximum temperature of the nanofluid rises to the volume fraction of 10 ppm, the maximum temperature of the collector reaches a constant value. A possible explanation for this would be the improvement of the thermal conductivity of the heat transfer fluid. It is the displacements and collisions between nanoparticles as a result of the Brownian motion due to the presence of nanoparticles in the working fluid. Increasing the nanoparticle concentration increases the number of nanoparticle molecules in the nanofluid, causing the

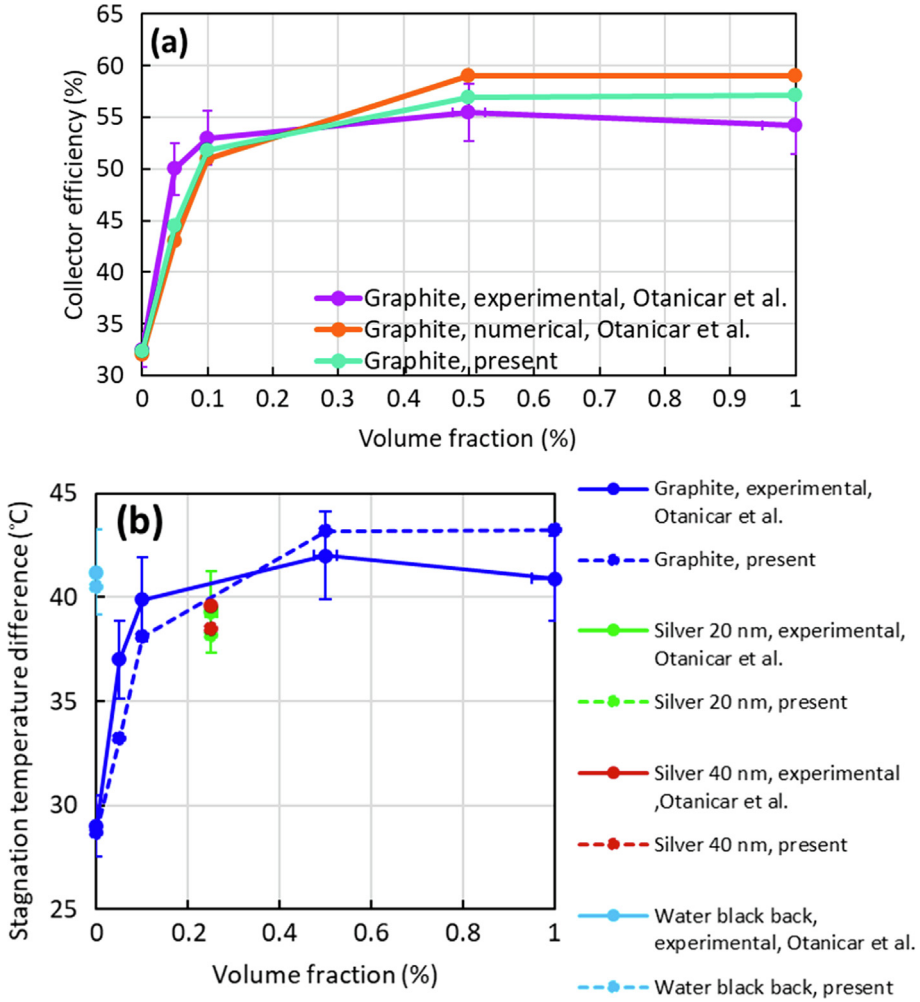

Fig. 4. Comparison of the efficiency and stagnation temperature difference results of the present study with benchmark [21].

Table 2
Comparison of results for mean Nusselt number with benchmark.

	Mean *Nu*, Al_2O_3-water (ϕ = 4 %)	
	Present	Ho et al. [62]
Ra =10^4	2.33	2.45
Ra =10^5	4.86	4.85
Ra =10^6	9.63	9.61

increase in the collisions and interfacial effects between the molecules and the surface volume ratio. This positive enhancement of Brownian motion, however, can be observed more at lower volume concentrations. This is because the nanofluid becomes more viscous with increasing nanoparticle concentration. Because this will limit the movement of nanoparticles in the nanofluid, it will reduce the collision of the molecules and cause the convection currents in the nanofluid to decrease.

As revealed in Fig. 6(a-g), the solar radiation begins to be absorbed by the nanoparticles in the collector from the edges,

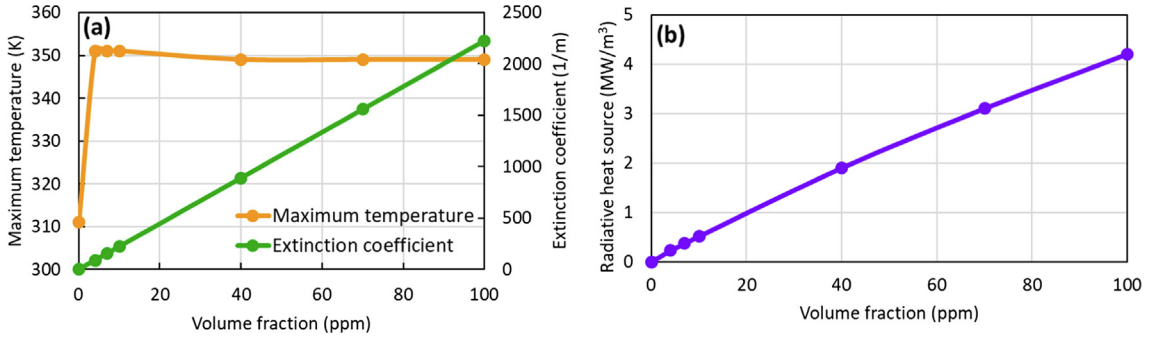

Fig. 5. (a) Extinction coefficient of Graphite/water nanofluid and maximum temperature of the nanofluid, and (b) the maximum volumetric heat generation by radiation within the collector with different volume fractions.

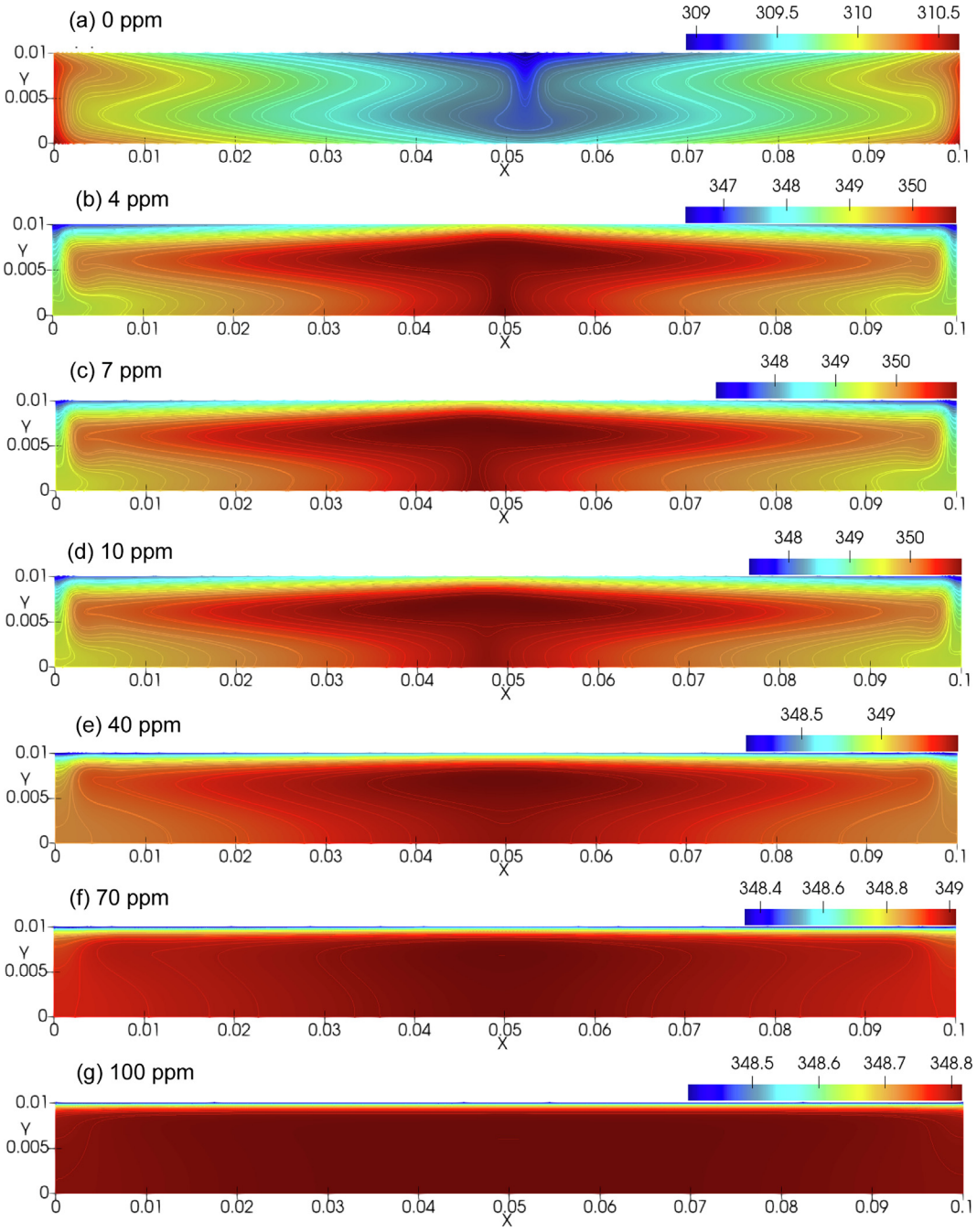

Fig. 6. Temperature (Kelvin, K) contours of Graphite/water nanofluid with different volume fractions of nanoparticles.

and the fluid begins to heat up. Because the bottom wall of the collector has a highly reflective feature, the incoming radiation is reflected inside the collector, and the nanofluid moves upwards due to thermal expansion. Additionally, Fig. 6(a-g) shows that the temperature distribution in the collector is more uniform with the increase in the nanoparticle volume fraction. As the irradiation penetrates the bottom of the collector, the base liquid layer absorbs this radiation, and as a result, a more uniform temperature distribution is obtained. However, the maximum radiative heat source or volumetric absorbed radiation (Wm^{-3}), which is the heat generation that occurs in the fluid when the radiation acts on the fluid, increases linearly with increasing the volume fraction of nanoparticles, see Fig. 5(b). In addition, the probability of light scattering increases because of the possibility of collision between the particles and light. Therefore, because of the weakening of light intensity, the radiative heat source within the collector gradually decreases with depth, as can be observed in Fig. 7(a-g).

However, Fig. 8(a-g) shows that with the increase of the volume fraction of the nanoparticles, vortices are formed and spread towards the inside of the collector, starting from the edges, and spreading to the corners due to the heating of the fluid from the edges. This situation can be explained by the effect of the buoyancy force by the temperature difference of the nanofluid. Because the increase in the volume concentration enhances the energy transfer of the nanofluids, an increase in the velocity of the fluid is observed. While the central vortex is dominant in the absence of the nanoparticle, its effect decreases with the increase in the volume concentration of the nanoparticle, taking the form of an

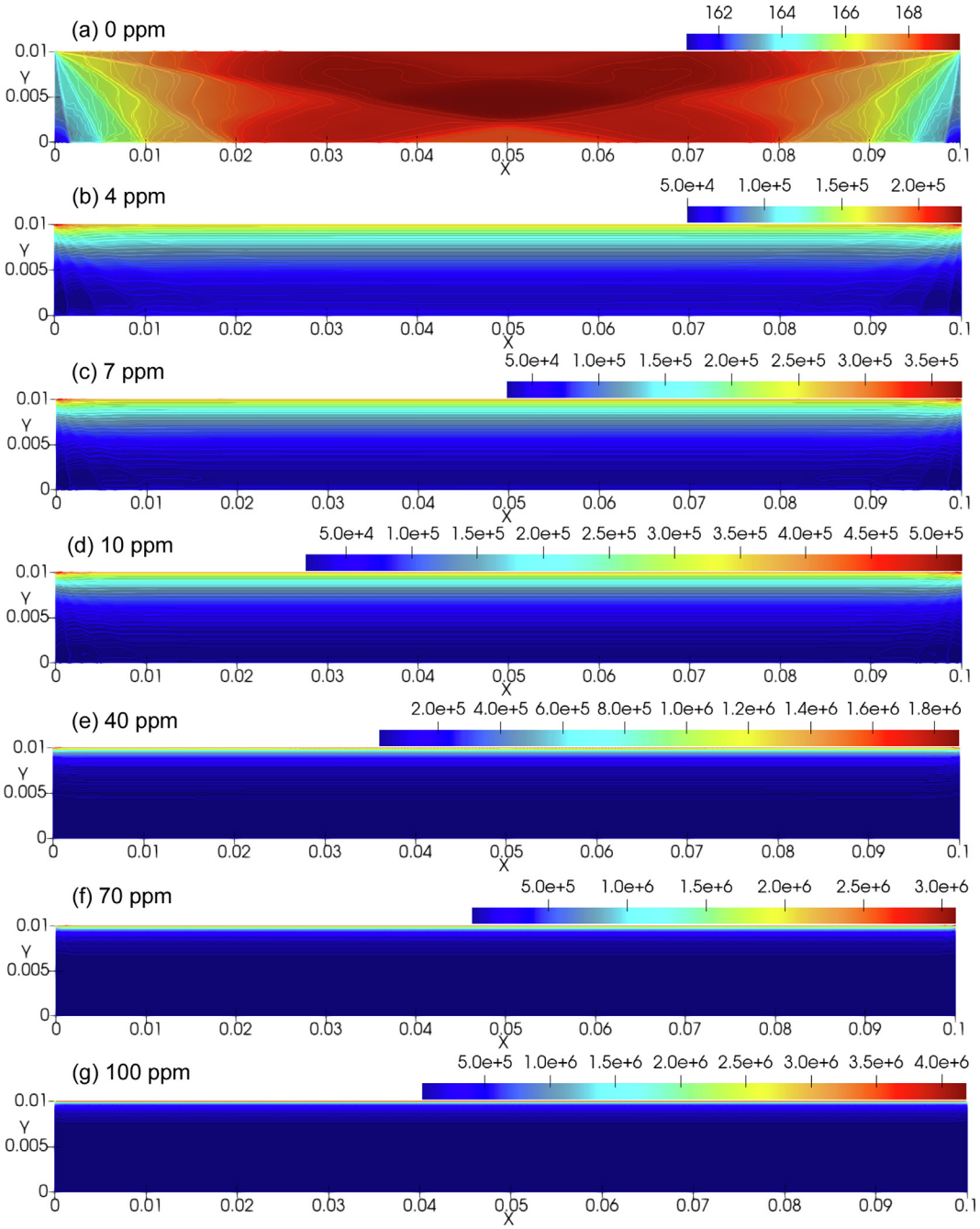

Fig. 7. Radiative heat source (Wm^{-3}) contours of Graphite/water nanofluid with for volume fractions nanoparticles.

ellipse and eventually disappears at 100 ppm (Figure (8(g))). In addition, an increase in the acceleration of the nanofluid is observed along the vertical walls and corners of the collector due to the increase of the boundary layers by decreasing the thickness in parallel with the increasing fraction.

4.2. Effects of nanoparticle type

In general, radiative and thermophysical properties of nanofluids vary with the nanoparticle. The effects of nanoparticle type are examined using Gold (Au), Copper (Cu), Graphite, Aluminium oxide (Al_2O_3), and Aluminium (Al) nanoparticles with different volume fractions of 4 ppm, 7 ppm, 10 ppm, 40 ppm, 70 ppm and 100 ppm. As the extinction coefficient of the nanofluid increases with increasing the volumetric fraction of nanoparticles, the nanofluid can absorb more solar radiation. Therefore, it improves the photothermal energy conversion by augmenting the heat that the collector can gain from solar energy increases, Fig. 9(b), and it improves the enthalpy difference that the collector can store as sensible heat, Fig. 9(a). As shown in Fig. 9, the improvement in Al/water and Al_2O_3/water nanofluids further increases by increasing the volumetric concentration of nanoparticles. In addition, thermal conductivity of the nanofluid is another factor affecting the thermal performance of the solar collector. As seen in Fig. 9, because the thermal conductivity of Graphite nanoparticles, which is a kind of carbon-based nanoparticle, is higher than other

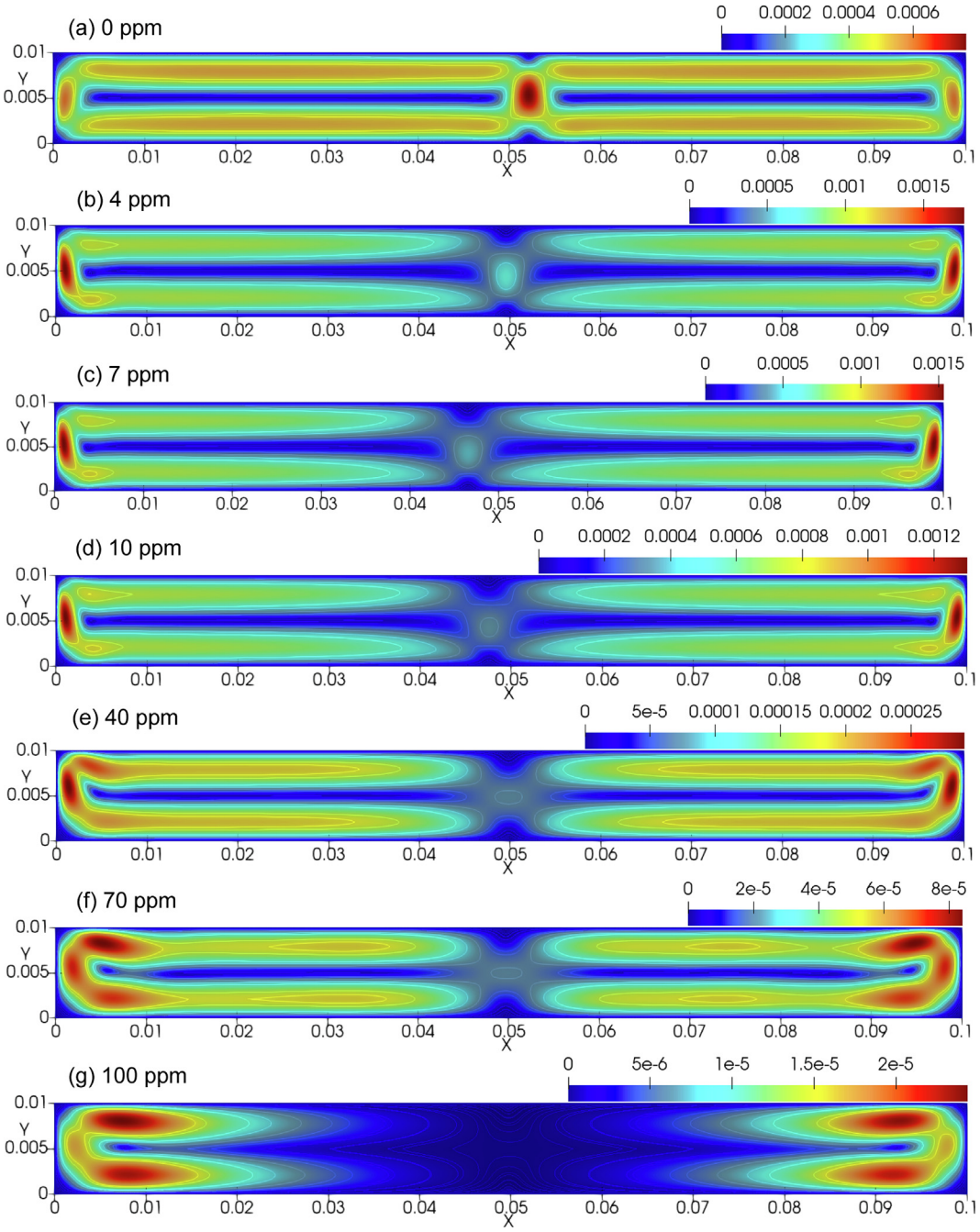

Fig. 8. Velocity (ms^{-1}) contours of Graphite/water nanofluid for different volume fractions of nanoparticles.

nanoparticles, it has been observed that its contribution to the thermal performance of the system is higher, especially at very low volume concentrations (4–10 ppm).

As the nanoparticles absorb more irradiation at the vicinity of the top wall, the top wall's radiation heat flux is higher than that of the other walls, as shown in Fig. 9(c). Furthermore, the addition of nanoparticles to the pure water enhances the sunlight capture of the heat transfer fluid. Therefore, the heat source produced by the radiation increases. As demonstrated in Fig. 9(d), the average volumetric heat generation is higher for the Graphite/water nanofluid than for the other types of nanofluid at all the volume concentrations considered. This is because the absorption capacity of the Graphite nanoparticle is higher than the other nanoparticles. Therefore, larger volumetric absorption by radiation occurs. As illustrated in both Fig. 9(c-d), the effect of radiation improves with increasing volume concentration.

As shown in Fig. 10(a-e), the temperature distribution inside the solar collector is different for each nanoparticle at the volume fraction of 7 ppm. The heating process by the solar irradiation starts from the bottom and the edges and is pushed upwards by buoyancy force to the inside of the collector. Because the upper wall is exposed to the atmosphere, heat loss occurs from both radiation and convection. Therefore, cooling takes place over the upper wall, and it becomes stronger in the upper edge corners. Indeed, the maximum temperature occurs on the sidewalls as the cooling effect penetrates deeper towards the centre of the collector for the Al_2O_3/water nanofluid (Fig. 10(e)). In addition, although two different temperature regions are seen by using Al/water nano-

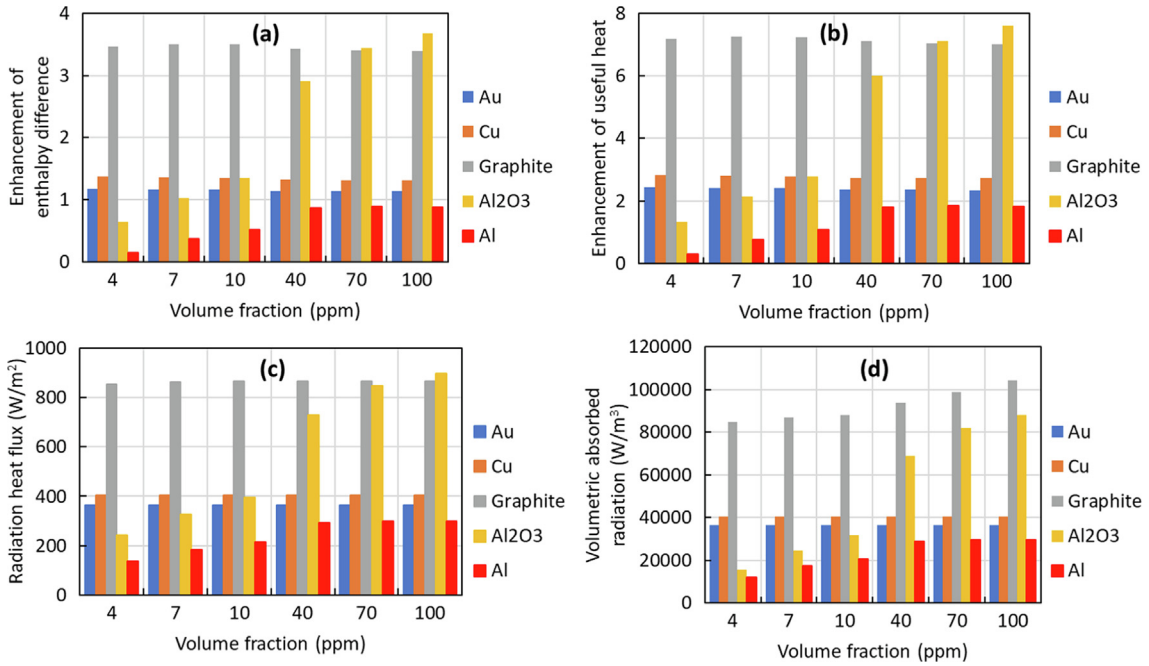

Fig. 9. Effect of different types of nanoparticles on the collector performance: (a) enhancement of enthalpy difference, (b) enhancement of useful heat, (c) radiation heat flux at top wall, and (d) volumetric heat generation by radiation within the collector with different volume fractions.

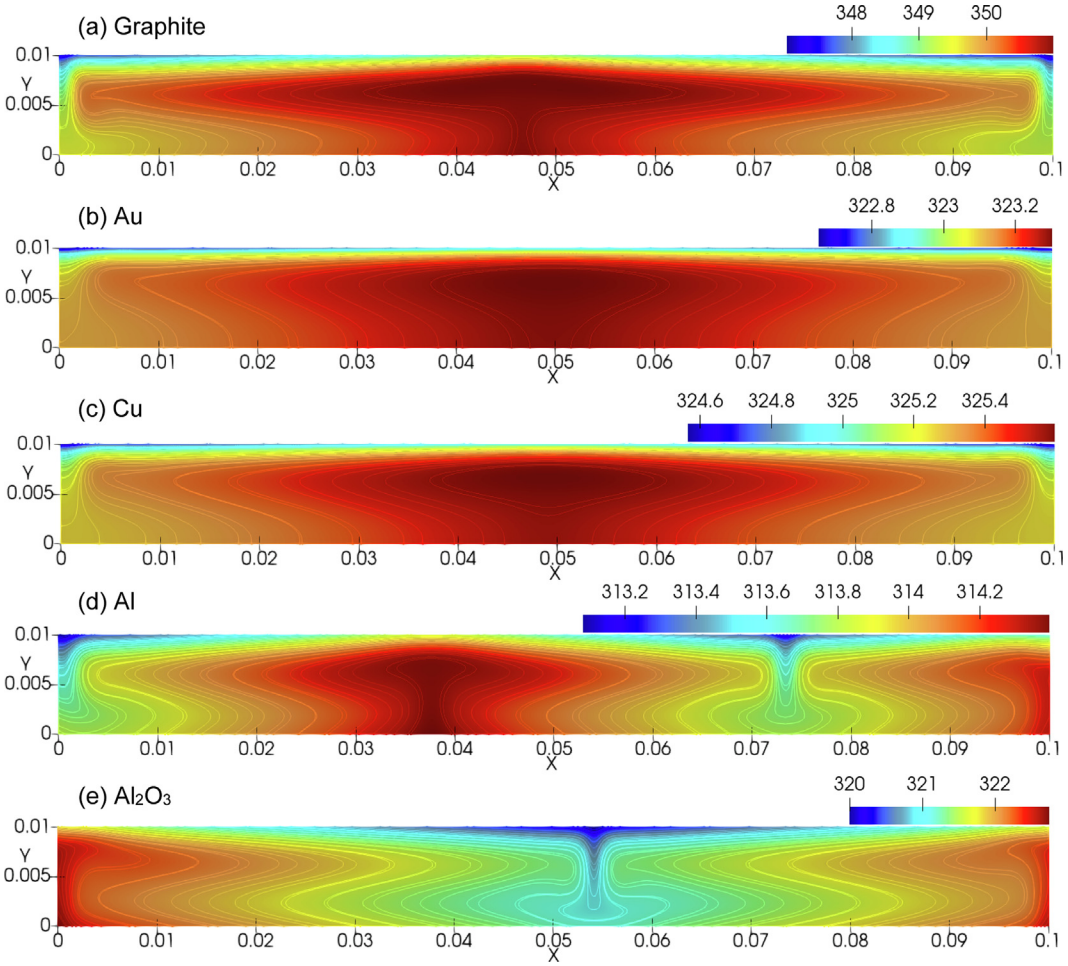

Fig. 10. Temperature (Kelvin, K) contours of water-based different nanofluids for volume fraction of 7 ppm.

fluid, the temperature difference is nearly uniform. Besides, a vortex formation of Al (Fig. 10(d)) and Al_2O_3 (Fig. 10(e)) nanoparticle-based nanofluids is observed from the top surface of the collector towards the inside. The reason for this is that the radiation absorption capacity is less compared to other nanoparticles, causing the increase in temperature gains to be less, it seems as if the cooling effect is more pronounced than other nanofluids.

4.3. Effects of hybrid nanofluid

With the addition of nanoparticles, the ability of the nanofluid to absorb solar radiation increases, and thus its transmittance is reduced. Consequently, the fluid temperature increases. The total extinction capacity of hybrid nanofluids depends on the extinction coefficient of each type of nanoparticle. Therefore, since hybrid

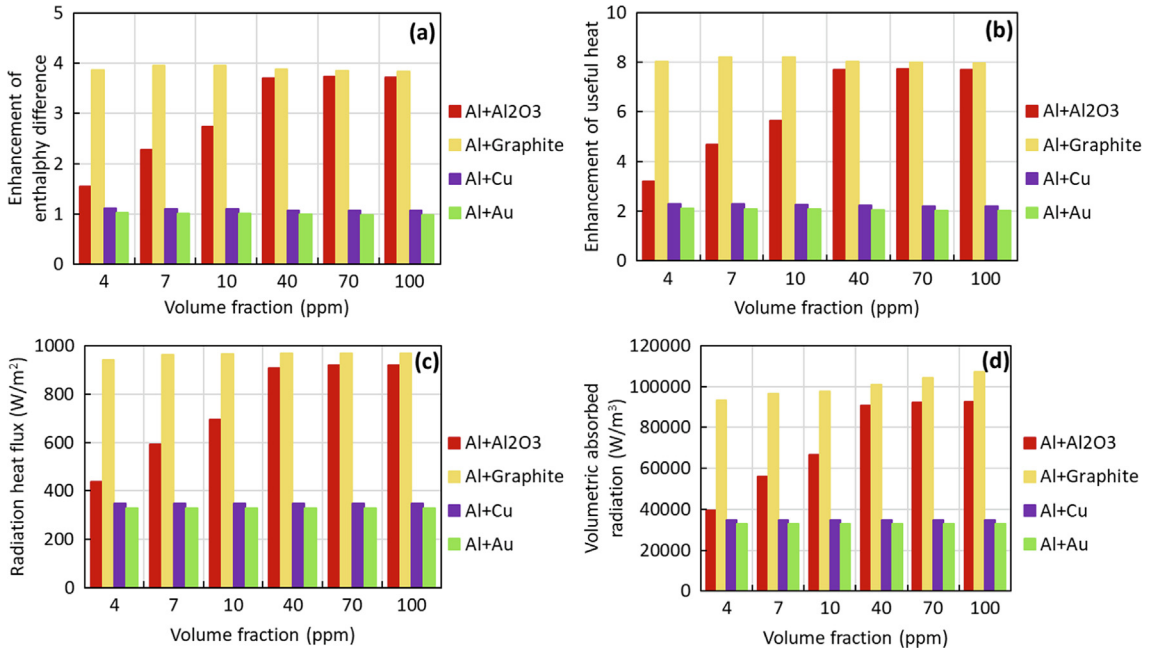

Fig. 11. Effect of different nanoparticles on the collector performance (a) enhancement of enthalpy difference, (b) enhancement of useful heat, (c) radiation heat flux at top wall, and (d) volumetric heat generation by radiation within the collector with different volume fractions.

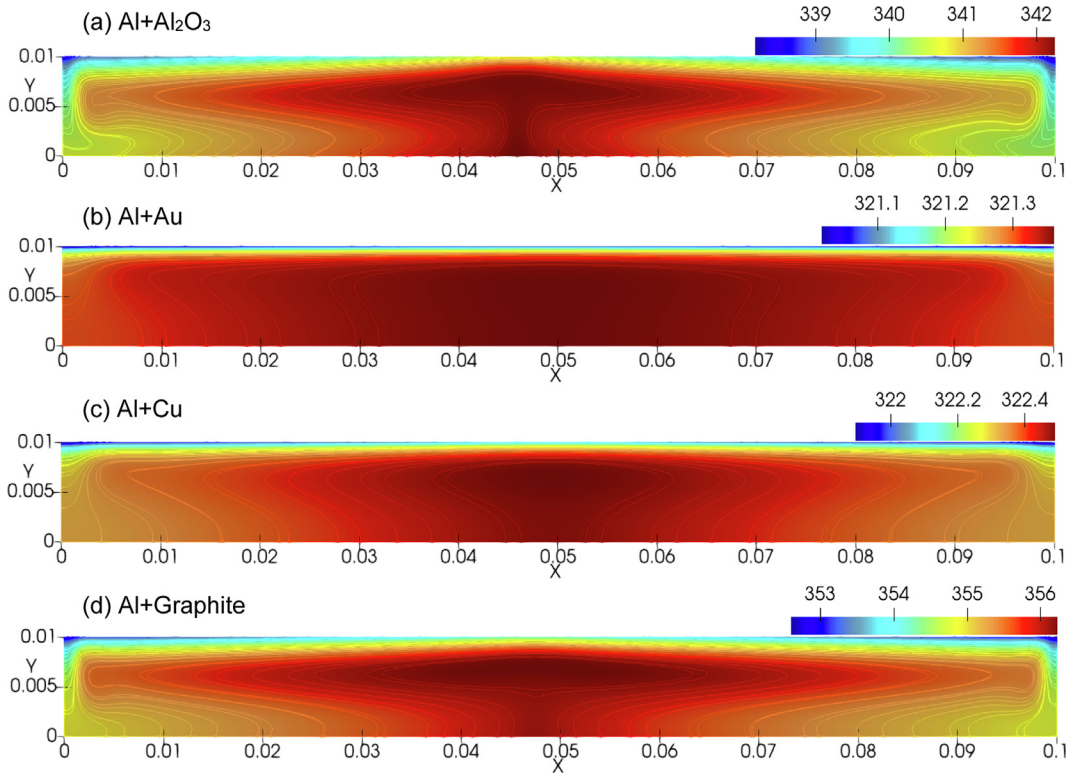

Fig. 12. Temperature (Kelvin, K) contours of water-based different nanofluids for volume fraction of 10 ppm.

nanofluids have the capacity to absorb more solar radiation, the temperature of the nanofluid increases and the performance of the solar collector increases. Al is chosen as the basic nanoparticle because it shows less thermal performance than other nanofluids in Fig. 9. When other nanoparticles (same shape and size) are added to the Al/water nanofluid, an enhancement is observed for each volumetric concentration, as shown in Fig. 11, because of the effects of hybrid nanoparticles. The temperature rises of Al + Al_2O_3 hybrid nanofluid are higher than those of Al nanofluid and Al_2O_3 nanofluid as shown in Fig. 10(d-e) and 12(a). However, other nanofluids have less effects on the temperature increase. When Au, Cu and Graphite nanofluids are added to the Al nanofluid, as shown in Fig. 12(a-d), the temperature of the hybrid nanofluid increases, but the maximum temperature of the hybrid nanofluid is not higher than the temperature of the nanofluids that constitute the hybrid nanofluid. However, Fig. 11(a-b) show that the thermal performance of hybrid nanofluids are higher than the mono nanofluids. Thus, with increasing temperature gain, the useful heat of the heat transfer fluid is improved by increasing the photothermal conversion performance (Fig. 11(b)), and so more heat can be stored with higher enthalpy gain (Fig. 11(a)). As the temperature differences in the collector of Al + Au and

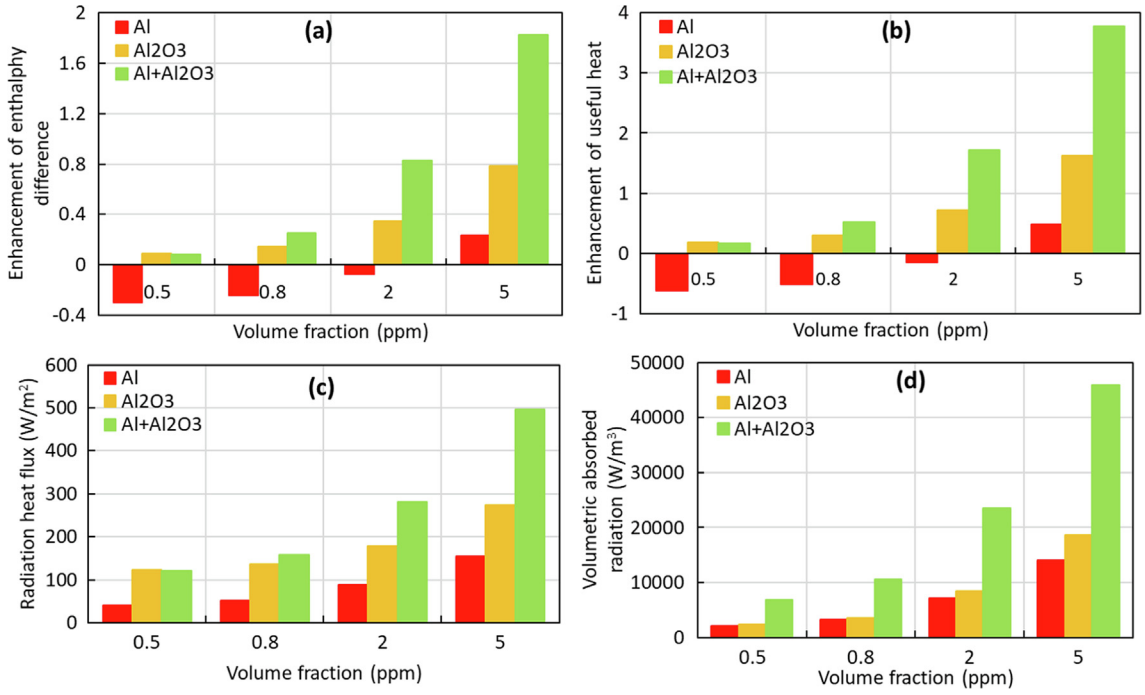

Fig. 13. Effects of different nanoparticles on the collector performance (a) enhancement of enthalpy difference, (b) enhancement of useful heat, (c) radiation heat flux at top wall, and (d) volumetric heat generation by radiation within the collector with different volume fractions.

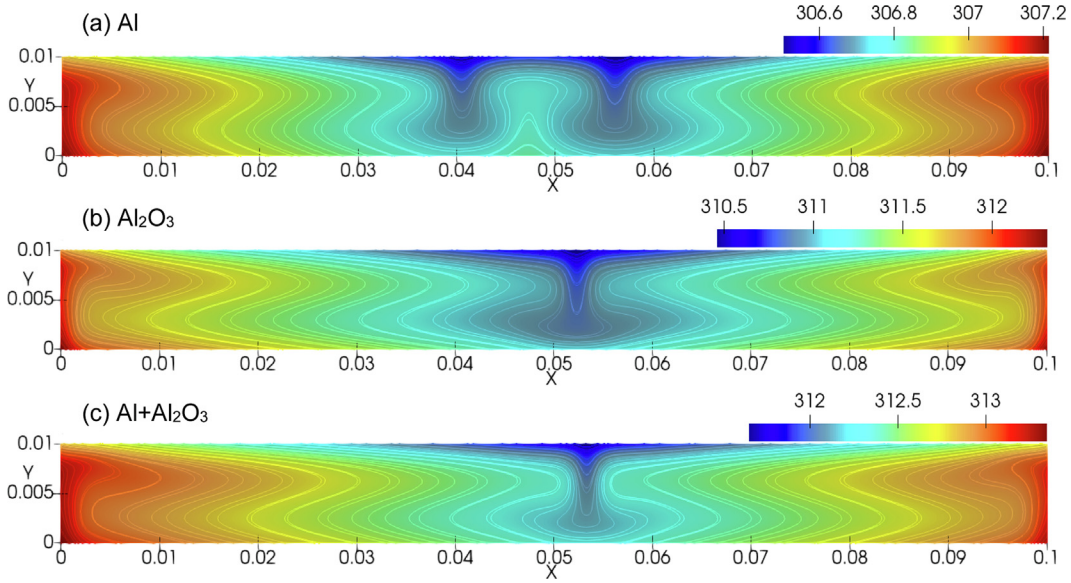

Fig. 14. Temperature (Kelvin, K) contours of water-based different nanofluids at volume fraction of 0.8 ppm.

Al + Cu hybrid nanofluids are approximately zero, the temperature distributions inside the collector are more uniform as shown in Fig. 12(b-c). In addition, because the added nanoparticles intensify the absorption of sunlight by the nanofluid, as shown in Fig. 11(d), the average volumetric absorption produced by the radiation inside the collector increases. Furthermore, as the nanoparticles close to the upper wall absorb more solar radiation, more radiative heat flux occurs at the upper wall, see Fig. 11(c). This photothermal conversion performance enhancement reflects those of Zhang et al. [19] who also demonstrated that hybrid nanoparticles enhance the light-to-heat conversion.

Since the inside of the solar collector is semi-transparent, the irradiation is absorbed by the fluid [63]. Therefore, the heat generated from the radiation in the collector is absorbed by the nanoparticles, causing the development of temperature profiles. This depends on the absorption co-efficient of nanoparticles, and the absorption coefficient increases as the concentration of nanoparticles increases. Using a certain concentration can cause radiation to be absorbed by nanoparticles. For the Al/water nanofluid, 0.5 ppm and 0.8 ppm volume concentrations have a negative effect on the collector performance by causing the temperature gradients not to develop as a result of their inability to absorb the radiation sufficiently by the nanoparticles. As seen in Fig. 13(a-b) because there is no sufficient heat gain, no increase in the temperature of the nanofluid is observed and there is a decrease in the collector performance. Because of the insufficient absorption, the top wall radi-

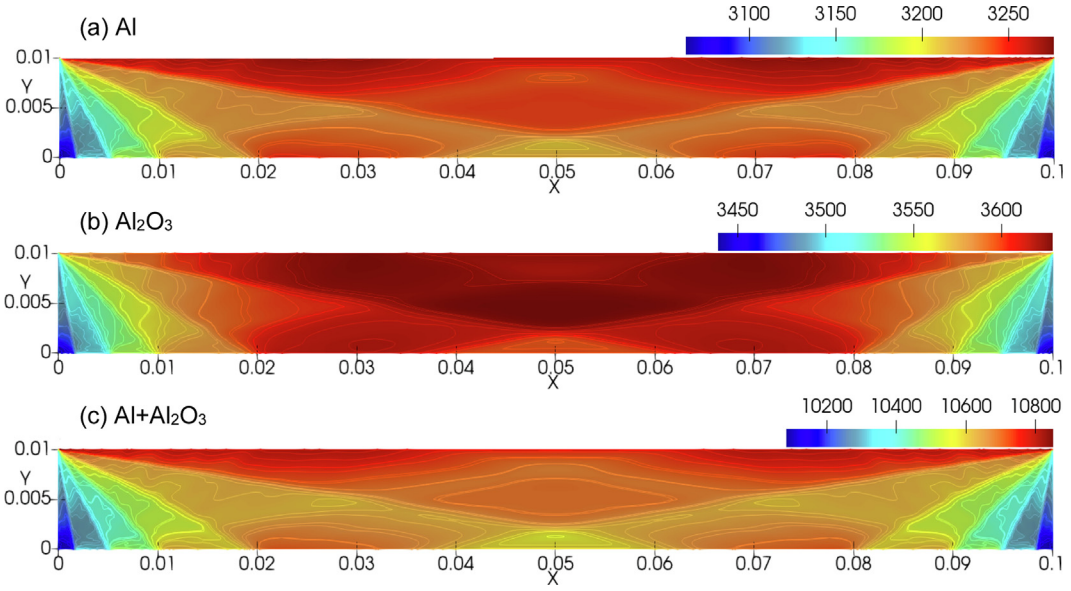

Fig. 15. Radiative heat source (Wm^{-3}) contours of water-based different nanofluids for volume fraction of 0.8 ppm.

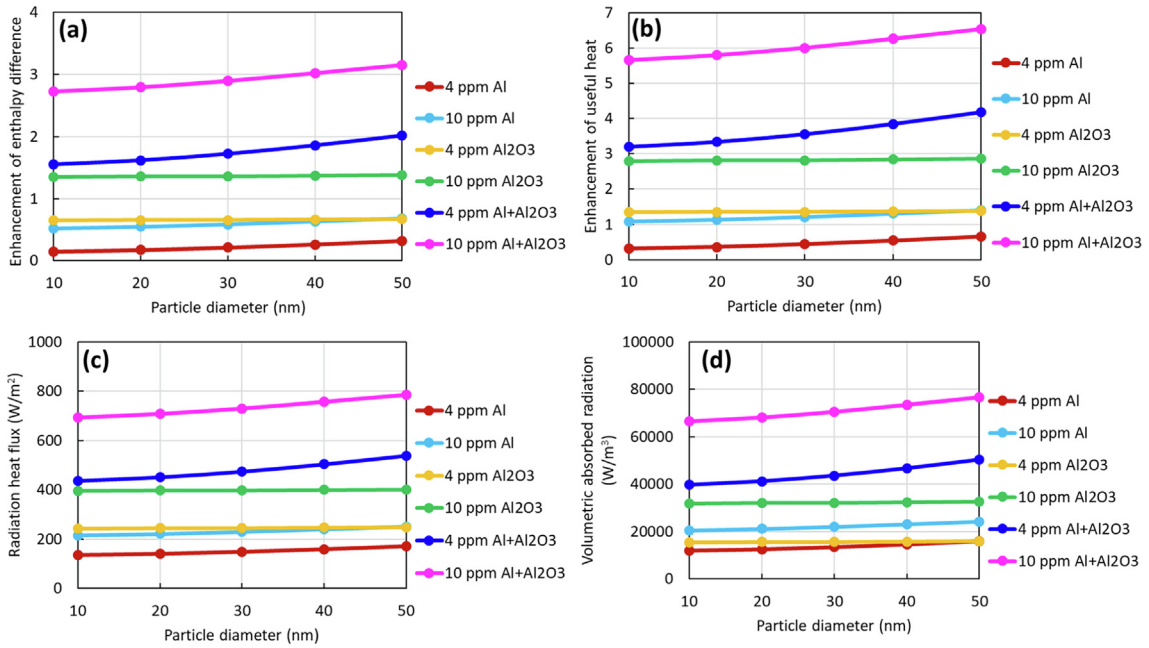

Fig. 16. Effects of different nanoparticles on the collector performance (a) enhancement of enthalpy difference, (b) enhancement of useful heat, (c) radiation heat flux at top wall, and (d) volumetric heat generation by radiation within the collector with different particle diameter.

ation heat flux for Al/water nanofluid is lower than pure water (104 W/m^2), and it enhances with increasing the volume concentration of nanoparticles as seen in Fig. 13(c). This result corroborates the views of Zhang et al. [20], who suggested that the enough volume concentration should be used in order to absorb adequate the irradiation. Fig. 14 shows that since the heat loss on the upper wall is higher in the Al/water nanofluid compared to other nanofluid types, the cooling effect is stronger. In addition, the volumetric heat generation of the Al/water nanofluid is minimal, as shown in Fig. 15(a), because Al nanoparticles at a volumetric concentration of 0.8 ppm poorly absorbs radiation, and the average volumetric heat generation increases with increasing the volume concentration (Fig. 13(d)).

As demonstrated in Fig. 14(a-c), heating starts at the sides and progresses towards the inside of the collector with the effect of the buoyancy force. In addition, heat loss occurs by a combination of radiation and convection from the upper wall to the ambient, resulting in large cold temperature gradients from the upper wall to the centre of the collector. Therefore, since the volume concentration of Al nanoparticles is below the minimum volume fraction (4 ppm in Fig. 9(a)), the temperature gain in the collector (Fig. 14(a)) is less than in pure water (Fig. 6(a)), due to the lack of radiation absorption. This results in the formation of two vortexes, showing that the cooling effect in the Al/water nanofluid is stronger than in the other nanofluids. Moreover, since Al nanoparticles at 0.8 ppm volumetric concentration absorb radiation poorly, as shown in Fig. 15(a), the volumetric heat generation by the Al/water nanofluid in the collector is minimum. Furthermore, although sunlight penetrates through the height of the collector, the heat generated from the radiation reduces towards the bottom of the collector (Fig. 15(a-c)) because the intensity of sunlight decreases with depth.

4.4. Effects of nanoparticle size

The extinction co-efficient of nanoparticles depends on the particle diameter [27]. As seen in Equations (11) and (12), while the absorption co-efficient changes with the square of the particle diameter $\left(D^2\right)$, the scattering co-efficient changes with the third power of the particle diameter $\left(D^3\right)$. Therefore, as the extinction

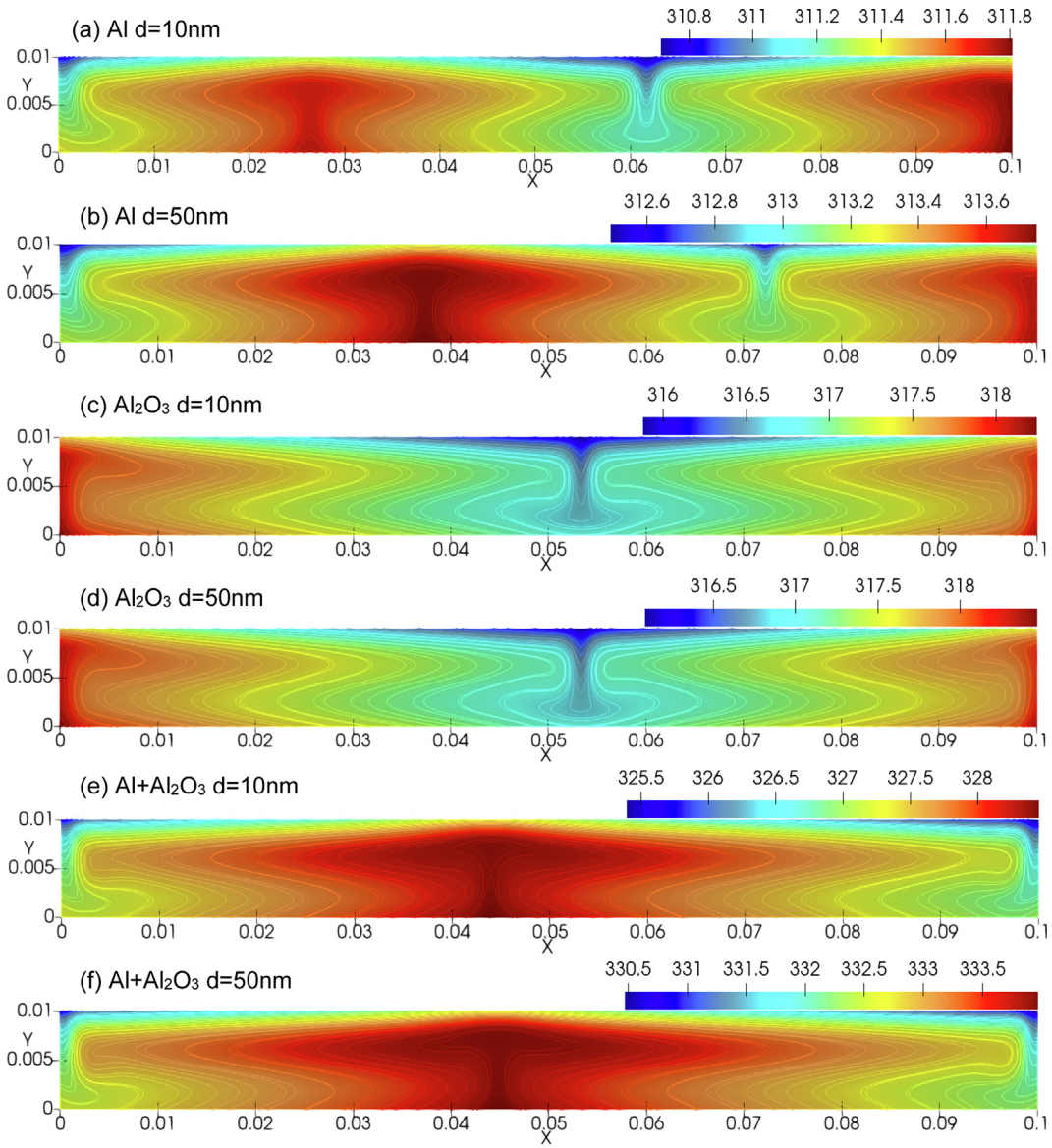

Fig. 17. Temperature (Kelvin, K) contours of water-based different nanofluids for volume fraction of 4 ppm.

coefficient improves with increasing particle size, the radiation absorption capacity of nanoparticles increases. This means that increasing the size of the nanoparticles contributes to the higher absorbance, resulting in an increase in the temperature of the nanofluid. These enhancement in temperature and absorption accelerate the heat distribution between nanoparticles and augment the photothermal conversion of the heat transfer fluid. With the increasing temperature and energy conversion, an increase is observed in the thermal performance of the collector as shown in Fig. 16(a-b). With the increase in particle size, an increase in the average volumetric absorption (Fig. 16(d)) and top wall heat flux (Fig. 16(c)) generated by the radiation is observed because of the improvement in the nanofluid. This is because the temperature rise increases with increasing nanoparticle diameter.

Fig. 17(a-f) demonstrates that as the Al + Al_2O_3/water nanofluid starts to heat up from the bottom of the collector, the effect of natural convection heat transfer is more visible. The heated fluid moves upwards from the centre of the bottom wall with the buoyancy force. Thus, it provides that there is more hot heat transfer fluid on the top wall of the collector. This contributes that the cold heat transfer fluid on the vicinity of the top wall moves downwards in the collector, reducing the heat loss from the collector to the ambient and ensuring that the temperature gain is higher than other nanofluids so that it is noticed that the vortex formation observed in mono nanofluids prevents this formation by blended nanofluids because of the higher temperature gain. In addition, the temperature increase in larger nanoparticles is greater than in smaller nanoparticles, as it increases the capacity to absorb sunlight. In other words, the optical performance of the heat transfer fluid enhances with the particle diameter. Hence, increasing the size of the nanoparticles contributes more to improving the temperature of the nanofluids as seen in Fig. 17(a-f).

Furthermore, as shown in Fig. 18(a-f), because the volumetric heat generation by radiation declines with the depth of cavity, the maximum radiation heat flux is obtained at the top wall. Thus, radiation heat flux and average volumetric absorbed radiation increase with increasing the nanoparticle diameter, as shown in Fig. 16(c-d). Moreover, Fig. 17(a, c, e) and 18(a, c, e) show that more uniform distributions are obtained from 10 nm nanoparticles as the maximum and minimum temperature and heat generation dif-

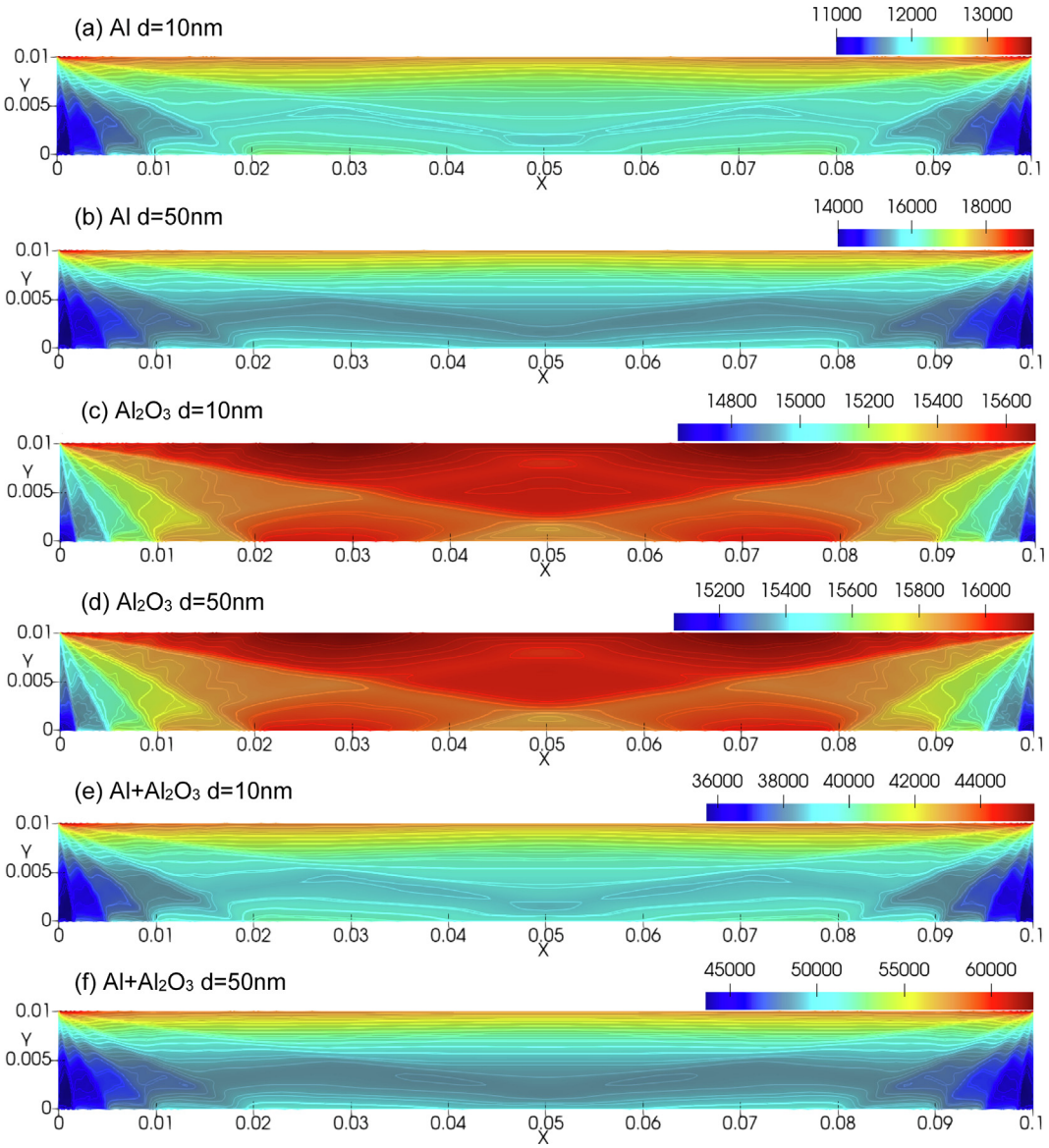

Fig. 18. Radiative heat source (Wm^{-3}) contours of water-based different nanofluids for volume fraction of 4 ppm.

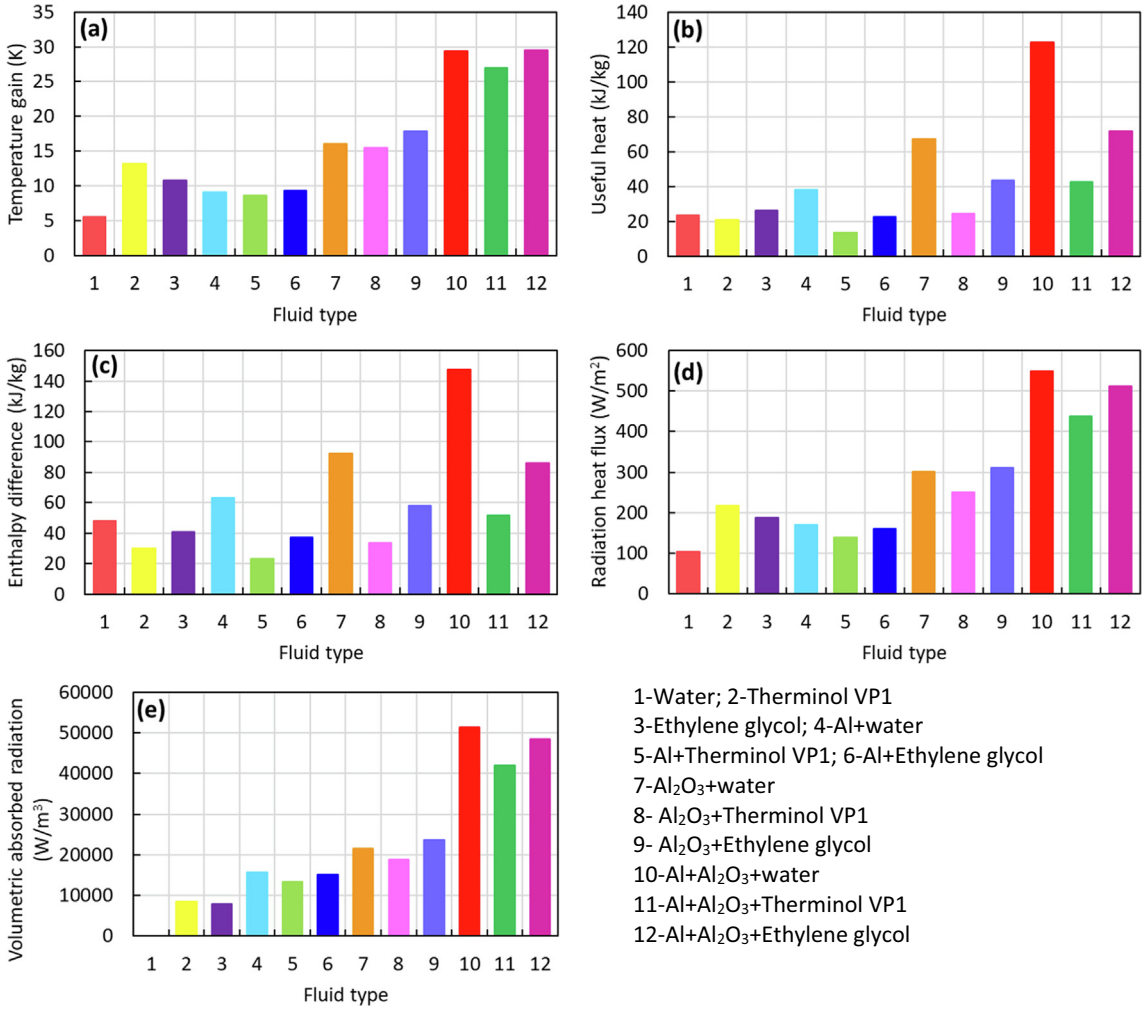

Fig. 19. Effects of different base fluid on the collector performance (a) temperature gain, (b) useful heat, (c) enthalpy difference, (d) radiation heat flux at top wall and (e) volumetric heat generation by radiation within the collector at volume fraction of 6 ppm.

ferences in the collector increase with increasing the size of nanoparticles. However, since the difference is very little in the Al_2O_3 nanofluid, the temperature and heat generation distributions remain almost the same.

4.5. Effects of base fluid types

The effect of the base fluid is investigated by using water, Therminol VP1 and ethylene glycol. Fig. 19(a) and (b) show that, despite the high temperature gain of Therminol VP1, the useful heat gain has the highest value among pure fluids because of the high specific value of ethylene glycol. The volumetric heat absorbed by the radiation depends on the temperature rise of the fluid. In addition, because the average temperature gains are close to each other in both fluids, the average volumetric heat generation is approximately the same. With the addition of nanoparticles, the thermal conductivity and absorption co-efficient of the fluid are improved. As a result of the hybrid nanoparticles being added to the pure fluids, a significant increase in the enthalpy difference is observed, see Fig. 19(c). Accordingly, the performance of the collector improves. As shown in Fig. 19(a), (d) and (e), there is a parallel relationship between the temperature increase in the collector and the effects of radiation on the collector. This is because the increase in temperature depends on the radiation absorption capacity of the pure fluids and nanoparticles. Therefore, the temperature increase is higher for hybrid nanoparticles and pure Therminol VP1 as a result of the high solar energy absorption capacity.

5. Conclusions

A directly heated solar collector was investigated numerically using different mono and hybrid nanoparticles in this study. The effects of nanoparticle size, base fluid and nanoparticle concentration were analysed to compare their effects upon the thermal performance of direct absorption solar collector enclosure. ANSYS Fluent was used to solve the 2D radiative heat transfer which includes scattering, emitting and absorption factors and energy equations. Numerical results show that as the radiation absorption capacity of the nanofluid increased, the average temperature of the fluid in the collector and the average volumetric heat generated by the radiation increased. Thus, the performance of the collector was enhanced. In addition, although the maximum radiative heat source increased linearly with increasing the volume concentration of nanoparticles, the radiative heat source within the collector gradually decreased with depth. Besides, increasing the volume concentration causes the nanoparticles at the vicinity of the upper wall to absorb more solar energy. Furthermore, when other nanoparticles were added to the Al/water nanofluid, an enhancement was observed for each volume concentration because of hybrid nanoparticles. The maximum enhancement of enthalpy dif-

ference was 3.74 and 3.96 for Al + Al_2O_3 and Al + Graphite nanoparticles with volume concentrations of 70 ppm and 10 ppm, respectively. The maximum enhancement of useful heat was also 7.74 and 8.20 for Al + Al_2O_3 and Al + Graphite nanoparticles with volume concentrations of 70 ppm and 10 ppm, respectively. Moreover, it was found that the collector performance enhances with increasing in particle diameter. More uniform distributions, however, were obtained from 10 nm nanoparticles as the maximum and minimum temperature and heat generation differences in the collector increased with increasing the particle size. Finally, although an increase in the nanoparticle concentration at the same particle diameter enhances the absorption of solar radiation by the nanofluid, since the viscosity of the nanofluids increases at high concentrations, the collisions between nanoparticles, which are the result of Brownian motion, are reduced. This causes a decrease in the thermal resistance of the interface between the nanoparticle molecules and the fluid, causing more photothermal conversion of the nanofluid to be prevented.

Considering the numerical results, discussions, and research gaps within the current study, it can be further concluded that hybrid nanofluids can be used both as a storage medium and a heat transfer fluid in direct absorption solar collectors, thus increasing the capturing and absorption capacity of the solar irradiation. Therefore, the photothermal conversion performance and sensible heat storage capacity of the heat transfer fluid is enhanced. Thanks to this improved thermal performance, hybrid nanofluids provide an inevitable advantage for solar energy applications.

Data availability

The data that support the findings of this study are available from the corresponding author upon reasonable request.

CRediT authorship contribution statement

Oguzhan Kazaz: Conceptualization, Methodology, Software, Validation, Investigation, Formal analysis, Visualization, Writing – original draft, Writing – review & editing. **Nader Karim:** Conceptualization, Supervision, Writing – review & editing. **Shanmugam Kumar:** Supervision, Writing – review & editing. **Gioia Falcone:** Supervision, Writing – review & editing. **Manosh C. Paul:** Conceptualization, Supervision, Writing – review & editing, Project administration, Resources, Funding acquisition.

Data availability

Data will be made available on request.

Declaration of Competing Interest

The authors declare that they have no known competing financial interests or personal relationships that could have appeared to influence the work reported in this paper.

Acknowledgments

The first author would like to thank the Turkish Ministry of National Education, Republic of Turkey for funding his PhD research study at the University of Glasgow.

References

[1] W. Li, X. Tian, X. Li, J. Liu, C. Li, X. Feng, C. Shu, Z.-Z. Yu, An environmental energy-enhanced solar steam evaporator derived from MXene-decorated cellulose acetate cigarette filter with ultrahigh solar steam generation efficiency, J. Colloid Interface Sci. 606 (1) (2022) 748–757.
[2] S. Ferahtia, H. Rezk, A.G. Olabi, H. Alhumade, H.S. Bamufleh, M.H. Doranehgard, M.A. Abdelkareem, Optimal techno-economic multi-level energy management of renewable-based DC microgrid for commercial buildings applications, Appl. Energy 27 (2022).
[3] Y. Ma, Z. Hu, N. Lu, Y. Niu, X. Deng, J. Li, Z. Zhu, H. Sun, W. Liang, A. Li, Highly efficient solar photothermal conversion of graphene-coated conjugated microporous polymers hollow spheres, J. Colloid Interface Sci. 623 (2022) 856–869.
[4] Q.-D. Ruan, L.-L. Liu, D.-H. Wu, J.-J. Feng, L. Zhang, A.-J. Wang, Cobalt phosphide nanoparticles encapsulated in manganese, nitrogen co-doped porous carbon nanosheets with rich nanoholes for high-efficiency oxygen reduction reaction, J. Colloid Interface Sci. 627 (2022) 630–639.
[5] A. Sohani, H. Sayyaadi, S.R. Miremadi, X. Yang, M.H. Doranehgard, S. Nizetic, Determination of the best air space value for installation of a PV façade technology based on 4E characteristics, Energy vol. 262, no. B (2023).
[6] M.R. Saffarian, M. Moravej, M.H. Doranehgard, Heat transfer enhancement in a flat plate solar collector with different flow path shapes using nanofluid, Renew. Energy 146 (2020) 2316–2329.
[7] A. Lenert, E.N. Wang, Optimization of nanofluid volumetric receivers for solar thermal energy conversion, Sol. Energy 86 (1) (2012) 253–265.
[8] D. Wang, Y. Jia, Y. He, L. Wang, J. Fan, H. Xie, W. Yu, Enhanced photothermal conversion properties of magnetic nanofluids through rotating magnetic field for direct absorption solar collector, J. Colloid Interface Sci. 557 (2019) 266–275.
[9] M. Bahiraei, S. Heshmatian, Graphene family nanofluids: A critical review and future research directions, Energ. Conver. Manage. 196 (2019) 1222–1256.
[10] A.H. Pordanjani, S. Aghakhani, M. Afrand, B. Mahmoudi, O. Mahian, S. Wongwises, An updated review on application of nanofluids in heat exchangers for saving energy, Energ. Conver. Manage. 198 (2019).
[11] D. Song, Y. Wang, D. Jing, J. Geng, Investigation and prediction of optical properties of alumina nanofluids with different aggregation properties, Int. J. Heat Mass Transf. 96 (2016) 430–437.
[12] M. Chen, Y. He, J. Zhu, D.R. Kim, Enhancement of photo-thermal conversion using gold nanofluids with different particle sizes, Energ. Conver. Manage. 112 (2016) 21–30.
[13] M. Du, G.H. Tang, Optical property of nanofluids with particle agglomeration, Sol. Energy 122 (2015) 864–872.
[14] Z. Said, R. Saidur, N.A. Rahim, Optical properties of metal oxides based nanofluids, Int. Commun. Heat Mass Transfer 59 (2014) 46–54.
[15] A. Menbari, A.A. Alemrajabi, Y. Ghayeb, Investigation on the stability, viscosity and extinction coefficient of CuO–Al2O3/Water binary mixture nanofluid, Exp. Therm Fluid Sci. 74 (2016) 122–129.
[16] Q. He, S. Wang, S. Zeng, Z. Zheng, Experimental investigation on photothermal properties of nanofluids for direct absorption solar thermal energy systems, Energ. Conver. Manage. 73 (2013) 150–157.
[17] M. Karami, M.A.A. Bahabadi, S. Delfani, A. Ghozatloo, A new application of carbon nanotubes nanofluid as working fluid of low-temperature direct absorption solar collector, Sol. Energy Mater. Sol. Cells 121 (2014) 114–118.
[18] A. Menbari, A.A. Alemrajabi, Y. Ghayeb, Experimental investigation of stability and extinction coefficient of Al2O3–CuO binary nanoparticles dispersed in ethylene glycol–water mixture for low-temperature direct absorption solar collectors, Energ. Conver. Manage. 108 (2016) 501–510.
[19] H. Zhang, H.-J. Chen, X. Du, G. Lin, D. Wen, Dependence of Photothermal Conversion Characteristics on Different Nanoparticle Dispersions, J. Nanosci. Nanotechnol. 15 (4) (2015) 3055–3060.
[20] L. Zhang, J. Liu, G. He, Z. Ye, X. Fang, Z. Zhang, Radiative properties of ionic liquid-based nanofluids for medium-to-high-temperature direct absorption solar collectors, Sol. Energy Mater. Sol. Cells 130 (2014) 521–528.
[21] T.P. Otanicar, P.E. Phelan, R.S. Prasher, G. Rosengarten, R.A. Taylor, Nanofluid-based direct absorption solar collector, J. Renewable Sustainable Energy 2 (3) (2010) 033102–033113.
[22] M. Turkyilmazoglu, Performance of direct absorption solar collector with nanofluid mixture, Energ. Conver. Manage. 114 (2016) 1–10.
[23] H.K. Gupta, G.D. Agrawal, J. Mathur, Investigations for effect of Al2O3–H2O nanofluid flow rate on the efficiency of direct absorption solar collector, Case Studies in Thermal Engineering 5 (2015) 70–78.
[24] M. Hatami, D. Jing, Optimization of wavy direct absorber solar collector (WDASC) using Al2O3-water nanofluid and RSM analysis, Appl. Therm. Eng. 121 (2017) 1040–1050.
[25] A.I. Alsabery, S. Parvin, M. Ghalambaz, A.J. Chamkha, I. Hashim, Convection Heat Transfer in 3D Wavy Direct Absorber Solar Collector Based on Two-Phase Nanofluid Approach, Appl. Sci. 10 (20) (2020) 7265.
[26] M. Hatami, D. Jing, Evaluation of wavy direct absorption solar collector (DASC) performance using different nanofluids, J. Mol. Liq. 229 (2017) 203–211.
[27] H. Tyagi, P. Phelan, R. Prasher, Predicted Efficiency of a Low-Temperature Nanofluid-Based Direct Absorption Solar Collector, J. Sol. Energy Eng. 131 (4) (2009) 041004–041007.
[28] T.B. Gorji, A.A. Ranjbar, A numerical and experimental investigation on the performance of a low-flux direct absorption solar collector (DASC) using graphite, magnetite and silver nanofluids, Sol. Energy 135 (2016) 493–505.
[29] M. Siavashi, K. Ghasemi, R. Yousofvand, S. Derakhshan, Computational analysis of SWCNH nanofluid-based direct absorption solar, Sol. Energy 170 (2018) 252–262.
[30] S. Delfani, M. Esmaeili, M. Karami, Application of artificial neural network for performance prediction of a nanofluid-based direct absorption solar collector, Sustainable Energy Technol. Assess. 36 (2019).

[31] "ANSYS Fluent User's Guide," ANSYS, Inc., Canonsburg, 2013.
[32] C.L. Tien, B. Drolen, Thermal radiation in particulate media with dependent and independent scattering, Annual review of numerical fluid mechanics and heat transfer 1 (1987) 1–32.
[33] S. Ladjevardi, A. Asnaghi, P.S. Izadkhast, A.H. Kashani, Applicability of graphite nanofluids in direct solar energy absorption, Sol. Energy 94 (2013) 327–334.
[34] M.A. Karim, O. Arthur, P.K. Yarlagadda, M. Islam, M. Mahiuddin, Performance investigation of high temperature application of molten solar salt nanofluid in a direct absorption solar collector, Molecules 24 (2) (2019) 285.
[35] G.M. Hale, M.R. Querry, Optical Constants of Water in the 200-nm to 200-μm Wavelength Region, Appl. Opt. 12 (3) (1973) 555–563.
[36] E. D. Palik, Handbook of Optical Constants of Solids, Academic Press, 1997.
[37] M. Bass, C. M. DeCusatis, J. M. Enoch, V. Lakshminarayanan, G. Li, C. MacDonald, V. N. Mahajan and E. V. Stryland, Handbook of Optics, Third Edition Volume IV: Optical Properties of Materials, Nonlinear Optics, Quantum Optics, 2009.
[38] L.G. Schulz, The Optical Constants of Silver, Gold, Copper, and Aluminum. I. The Absorption Coefficient k, J. Opt. Soc. Am. 44 (5) (1954) 357–362.
[39] L.G. Schulz, F.R. Tangherlini, Optical Constants of Silver, Gold, Copper, and Aluminum. II. The Index of Refraction n, J. Opt. Soc. Am. 44 (5) (1954) 362–368.
[40] C. F. Bohren and D. R. Huffman, Absorption and Scattering of Light by Small Particles, New York: Wiley, 1983.
[41] H.M.F. Rabbi, A.Z. Sahin, B.S. Yilbas, A. Al-Sharafi, Methods for the determination of nanofluid optical properties: A review, Int. J. Thermophys. 42 (9) (2021) 1–42.
[42] S. Dugaria, M. Bortolato, D.D. Col, Modelling of a direct absorption solar receiver using carbon based nanofluids under concentrated solar radiation, Renew. Energy vol. 128, no. B (2018) 495–508.
[43] P. Ternik, Conduction and convection heat transfer characteristics of water–Au nanofluid in a cubic enclosure with differentially heated side walls, Int. J. Heat Mass Transf. 80 (2015) 368–375.
[44] K. Khanafer, K. Vafai, M. Lightstone, Buoyancy-driven heat transfer enhancement in a two-dimensional enclosure utilizing nanofluids, Int. J. Heat Mass Transf. 46 (19) (2003) 3639–3653.
[45] B. Ghasemi, S.M. Aminossadati, Periodic natural convection in a nanofluid-filled enclosure with oscillating heat flux, Int. J. Therm. Sci. 49 (1) (2010) 1–9.
[46] O.Z. Sharaf, A.N. Al-Khateeb, D.C. Kyritsis, E. Abu-Nada, Direct absorption solar collector (DASC) modeling and simulation using a novel Eulerian-Lagrangian hybrid approach: Optical, thermal, and hydrodynamic interactions, Appl. Energy 231 (2018) 1132–1145.
[47] R. Kaluri, S. Vijayaraghavan, S. Ganapathisubbu, Model Development and Performance Studies of a Concentrating Direct Absorption Solar Collector, J. Sol. Energy Eng. 137 (2) (2015).
[48] J. A. Duffie and W. A. Beckman, Solar Engineering of Thermal Processes, New Jersey: John Wiley & Sons, Inc., Hoboken, 2013.
[49] T. Basak, A.J. Chamkha, Heatline analysis on natural convection for nanofluids confined within square cavities with various thermal boundary conditions, Int. J. Heat Mass Transf. 55 (21–22) (2012) 5526–5543.
[50] R.S.R. Gorla, S. Siddiqa, M.A. Mansour, A.M. Rashad, T. Salah, Heat Source/Sink Effects on a Hybrid Nanofluid-Filled Porous Cavity, J. Thermophys Heat Transfer 31 (4) (2017) 847–857.
[51] R.L. Hamilton, O.K. Crosser, Thermal Conductivity of Heterogeneous Two-Component Systems, Industrial andEngineering Chemistry Fundamentals 1 (3) (1962) 187–191.
[52] S.S.U. Devi, S.P. Anjali Devi, Numerical investigation of three-dimensional hybrid Cu–Al2O3/water nanofluid flow over a stretching sheet with effecting Lorentz force subject to Newtonian heating, Can. J. Phys. 94 (5) (2016) 490–496.
[53] Y. Xuan, Q. Li, W. Hu, Aggregation Structure and Thermal Conductivity, AIChE J 49 (2003) 1038–1043.
[54] B.C. Pak, Y.I. Cho, Hydrodynamic and heat transfer study of dispersed fluids with submicron metallic oxide particle, Exp. Heat Transfer 11 (2) (1998) 151–170.
[55] R.R. Sahoo, J. Sarkar, Heat transfer performance characteristics of hybrid nanofluids as coolant in louvered fin automotive radiator, Heat Mass Transf. 53 (2017) 1923–1931.
[56] H. Moghadasi, E. Aminian, H. Saffari, M. Mahjoorghani, A. Emamifar, Numerical analysis on laminar forced convection improvement of hybrid nanofluid within a U-bend pipe in porous media, Int. J. Mech. Sci. 179 (2020).
[57] B. Takabi, S. Salehi, Augmentation of the heat transfer performance of a sinusoidal corrugated enclosure by employing hybrid nanofluid, Adv. Mech. Eng. 6 (2014).
[58] Y. Cengel and M. Boles, Thermodynamics: An Engineering Approach, 2015.
[59] Y. Zhou, Q. Li, Q. Wang, Energy Storage Analysis of UIO-66 and Water Mixed Nanofluids: An Experimental and Theoretical Study, Energies 12 (13) (2019) 2521.
[60] L. Zhang, R. Li, B. Tang, P. Wang, Solar-thermal conversion and thermal energy storage of graphene foam-based composites, Nanoscale 8 (2016) 14600–14607.
[61] M. F. Modest, Radiative Heat Transfer, Academic Press, 2013.
[62] C. Ho, M.W. Chen, Z.W. Li, Numerical simulation of natural convection of nanofluid in a square enclosure: Effects due to uncertainties of viscosity and thermal conductivity, Int. J. Heat Mass Transf. 51 (17–18) (2008) 4506–4516.
[63] R. Siegel, Transient Thermal Effects of Radiant Energy in Translucent Materials, J. Heat Transfer 120 (1) (1998) 4–23.